Composites Communications 54 (2025) 102258

Contents lists available at ScienceDirect

Composites Communications

journal homepage: www.elsevier.com/locate/coco

Short Review

Cellulose nanocrystals-based nanocomposites for sustainable energy storage technologies: From aligned microstructures to tailored performances

Jing Wang [a,b,*], Yue-E Miao [c,**]

[a] Department of Materials Science & Metallurgy, University of Cambridge, 27 Charles Babbage Road, Cambridge, CB3 0FS, United Kingdom
[b] Department of Mechanical Engineering, Swansea University, Bay Campus, Fabian Way, Swansea, SA1 8EN, United Kingdom
[c] State Key Laboratory for Modification of Chemical Fibers and Polymer Materials, College of Materials Science and Engineering, Donghua University, Shanghai, 201620, People's Republic of China

ARTICLE INFO

Keywords:
Sustainability
Next-generation energy storage
cellulose nanocrystals
Tailored alignment

ABSTRACT

The fast-moving development of emerging portable electronics and the rise of electric transportation with smart grids promote the ever-growing demand for sustainable, environmentally friendly, safe and large-scale electrochemical energy storage technologies. Notwithstanding lithium-ion batteries (LIBs) have dominated the current market as commonly used energy storage devices, the limited resources of lithium and the soaring costs have greatly restricted their long-lasting applications in the future. Therefore, sodium-ion, potassium-ion, and sodium-metal batteries have emerged as promising next-generation energy storage systems due to their abundance and cost-effectiveness. This review explores the transformative potential of cellulose nanocrystals (CNCs), derived from renewable biomass, as sustainable and high-performance materials for these emerging battery technologies. CNCs exhibit exceptional mechanical properties, biodegradability, and scalability, positioning them as ideal candidates for reinforcing electrodes and separators in nanocomposites. Herein, particular emphasis is placed on designing and fabricating aligned microstructures using appealing strategies such as unidirectional ice-templating and highly aligned electrospinning, which can tailor enhanced electrochemical performance and stability. By integrating CNC-based nanocomposites with the tailored aligned microstructures into battery designs, this unique review highlights principles, research progress and advancements that pave the way toward sustainable, safe, low-cost, efficient, and scalable energy storage solutions for a net-zero-emission future and circular economy.

1. Introduction

In line with the Paris Climate Agreement, adopted in 2015 [1], a total of 131 countries announced and agreed to implement national net-zero targets; these bring all greenhouse gas emissions to net zero by 2050 to stabilise global mean temperature [2]. However, an analysis of countries' current commitments and actions to reach GHG emission neutrality has concluded that they are insufficient to meet the goal of the Paris Agreement to limit the increase in global mean temperature to well below 2 °C while pursuing efforts to limit it further to 1.5 °C above pre-industrial levels [3,4]. Currently, the concept of carbon neutrality, which is defined as carbon dioxide (CO_2) emissions from all anthropogenic sources being net-zero, has gained considerable attention among policymakers and researchers, and increasingly governments of parties have formulated neutrality targets [5]. Notably, the global climate change crisis is substantially associated with CO_2 emissions stemming from the excessive use of carbon-based fossil fuels, accompanied by the acceleration of energy consumption for transportation, lighting, heating, and cooling in the twenty-first century [6]. Therefore, a viable and long-term solution to future a net-zero emission energy system is decarbonising by electrifying and generating electricity from renewable sources (*e.g.*, wind, solar, tidal, geothermal) as a substitute for carbon-based fossil fuel power generation [7]. Owing to the intermittent nature of renewable clean energy, the efforts to research and develop

* Corresponding author. Department of Mechanical Engineeriing, Swansea University, Bay Campus, Fabian Way, Swansea, SA1 8EN, United Kingdom.
** Corresponding author. State Key Laboratory for Modification of Chemical Fibers and Polymer Materials, College of Materials Science and Engineering, Donghua University, Shanghai, 201620, People's Republic of China.
E-mail addresses: jing.wang@swansea.ac.uk (J. Wang), yuee_miao@dhu.edu.cn (Y.-E. Miao).

https://doi.org/10.1016/j.coco.2025.102258
Received 6 December 2024; Received in revised form 3 January 2025; Accepted 5 January 2025
Available online 16 January 2025

energy storage devices and technologies (*e.g.*, rechargeable batteries, *etc.*) need to be pursued synchronously to achieve an efficient, reliable and affordable emission-free energy system.

Currently, fossil fuel depletion and CO_2 emission concerns accompanied by global warming issues have accelerated the development of mid- and large-scale rechargeable batteries for the development of emerging electric vehicles and grid-scale storage markets [8]. It is worth noting that electric vehicle sales have already exceeded a million units per year and are projected to grow markedly to reach about 30 million units per year by 2030, driven by increasing reliance on renewable energy sources and growth in demand for carbon-neutral and emissions-free energy storage devices with better performance (*i.e.*, lower costs and/or high energy density) [9]. The cost of current lithium-ion batteries (LIBs) is about US$150 k Wh^{-1} and energy density has further been raised to ~265 Wh kg^{-1} [10], making them the prevailing high-energy-density technology [11]. Today, LIB technology dominates the energy storage landscape from portable electronics (*e.g.*, mobile phones, laptops, *etc.*) to the rapidly expanding transportation market (*e.g.*, e-scooters, electric bicycles and vehicles, autonomous aircraft, *etc.*) [12,13].

Nevertheless, the limited reserve and uneven geo-distribution of lithium (20 ppm) resources (see Fig. 1) within the Earth's crust greatly constrain the applications of LIBs in large-scale energy storage systems [14,15]. This phenomenon propels an ever-growing demand for alternative post-LIBs as alternative systems to replace current systems, due to the present requirements of further reducing costs and increasing energy density. Considering the abundance of sodium (23 000 ppm) and potassium (17 000 ppm) in the Earth's crust, sodium- and potassium-ion batteries (SIBs/PIBs) have gained intensity as a topic of research due to their competitive cost and low redox potential (−2.71 V for Na^+/Na, −2.93 V for K^+/K and −3.04 V for Li^+/Li *vs.* standard hydrogen electrode (SHE)) [16]. In addition, SIBs and PIBs share identical rocking-chair mechanisms that Na/K ions rock forth and back between the intercalation-type electrodes during charge/discharge cycles, with that of LIBs based on the ions in the same alkali metal group. Consequently, from a manufacturing perspective, SIBs/PIBs can be industrialized using similar infrastructure and manufacturing machinery to conventional LIBs; meanwhile, the electrode architecture and cell design could be readily transferred from LIBs to SIBs/PIBs. Generally, electrode (*i.e.*, anode and cathode) materials, separators and electrolytes are core components of sodium/potassium-ion batteries.

Unfortunately, the commonly used graphite anode for LIBs is not appropriate for SIBs/PIBs; it is difficult to find suitable anode materials to accommodate the repeated insertion/extraction in a stable manner of the larger-sized Na-ion (1.02 Å) and K-ion (1.38 Å) in comparison to that of Li^+ (0.76 Å) [18,19]. Additionally, the insertion of larger ions into the anode material could lead to slow kinetics and a significant volume expansion/contraction during charge-discharge cycles, resulting in unsatisfactory rate capability and poor cycling performance [20]. Among numerous anode materials, hard carbons are one of the most promising choices for next-generation battery technologies beyond lithium due to their high reversible capacities. Nevertheless, most hard carbon materials are obtained by directly carbonizing natural precursors, and the obtained structural features without rational design cannot fully meet the specific requirements of storing sodium or potassium ions at the same time. Therefore, engineering the carbon structures by developing a controllable method is an urgent and challenging area of research for the further development of sodium- and potassium-ion batteries. Meanwhile, some reported hard carbons are fabricated from fossil fuels rather than renewable resources, which also hinders their overall sustainability.

Moreover, driven by the forecasted growth of the electric vehicles market, the other pivotal issue of each post-LIB technology for competitive industrial application is to lengthen the driving range of all-electric vehicles including hybrid electric vehicles, plug-in hybrid electric vehicles and electric vehicles; this will enable a reduction in the dependence on fossil fuels [21]. A promising solution toward higher energy density is substituting the insertion-type anodes in SIBs/PIBs such as carbonaceous materials with Na metal. Notably, sodium metal holds considerable promise as an anode material due to it being abundant, having a high theoretical capacity (1165 mAh g^{-1}), and low redox potential (−2.714V *vs.* a standard hydrogen electrode). Therefore, sodium-metal batteries (SMBs) are deemed to be one of the most promising high-energy and low-cost energy storage systems for next-generation large-scale applications [22,23]. However, the major impediments to the development of SMBs are associated with the

Fig. 1. The global distribution of Li resources until 2019. The amounts in each location are proportional to the circle areas. Reprinted with permission from Ref. [17] (Copyright © 2021, Springer Nature).

uncontrolled dendrite growth formed during Na plating/stripping, a degradation of battery cycle life, a battery short-circuiting, and eventually fire and tragedies when Na dendrites penetrate the separator to reach the cathode [24]. It is noteworthy that most long-term stable sodium metal anodes are evaluated in ether-based electrolytes. Carbonate-based electrolytes are the existing commercial and widely used choice for lithium-ion/-metal batteries due to their low cost and better oxidation stability that allows for high-voltage cathode materials. Nevertheless, there are few reports about the long cycle life of SMBs in carbonate-based electrolytes, owing to a higher reduction potential compared to ether-based electrolytes. Therefore, it is a challenging area of research to achieve the long-term cycling stability of SMBs in low-cost carbonate-based electrolytes.

2. Definitions, strategies, and applications

The progress of developing the advanced and low-cost SIBs/PIBs faces key challenges in finding appropriate anode materials to store Na^+/K^+ quickly and stably for tailoring the satisfactory rate and cycling capability. Materials sustainability is also an overriding factor in large-scale applications of SIBs/PIBs as next-generation sustainable batteries. Hard carbon derived from biomass as non-graphitic carbon with larger interlayer spacing and disordered structures has attracted numerous research interests as a potential anode material [25–27]. As an appealing alternative to non-biodegradable graphene and carbon nanotubes (CNTs) [28], cellulose nanocrystals (CNCs) that were extracted from biomass possess additional merits of biodegradability, sustainability, and scale-up availability with cost-competitiveness, which can be used as nano-reinforcements of nanocomposites due to their high Young's modulus. Therefore, CNCs-derived porous aerogels as sustainable and mechanical templates have been reported in considerable literature [29–31], allowing the fabrication of well-ordered structures by a unidirectional ice-templating strategy.

In this review, the relative definition, working principles, strategies and recent research progress on post-lithium-ion batteries using plants-derived CNCs as precursors as electrodes and separators of SIBs, PIBs and SMBs are summarised, in pursuit of sustainable post-lithium-ion technologies with low cost, high performance, and safety properties to avoid catastrophic battery incidents. Furthermore, this review provides a deeper understanding of how aligned microstructures can be engineered to control cellulose nanocrystal-based nanocomposites and subsequently tailor their electrochemical performance for next-generation batteries. While many post-lithium-ion technologies are being manufactured at a laboratory or pilot scale, the review presented herein is devoted to the rational design and fine-tuning of key components (*i.e.*, electrodes, separators) with favourable performances *via* processing-structure-property disciplines using CNCs-based nanocomposites for substituting current LIBs for industrial-scale manufacturing of post-lithium-ion batteries to realize the net-zero emission energy systems in the near future.

2.1. Cellulose nanocrystals

2.1.1. Structure of cellulose

Cellulose is one of the most abundant natural biopolymers on earth with an estimated annual production of about 1.5×10^{12} tons [32]; it can be extracted from plants including flax, cotton, ramie, hemp, jute, trees/plant, algae, or it can be generated by other non-plant sources such as bacteria and tunicates (sea squirts) [33,34]. Hence, cellulose is a vital renewable, biodegradable, and biocompatible material, and is increasingly being regarded as a green and environmentally friendly alternative to fossil-fuel-based polymers. In 1838, the first discovery of the isolation of cellulose from plant material was reported by the French Chemist Anselme Payen, and a committee that reviewed his work coined the term 'cellulose' [35]. Cellulose is a linear-chain carbohydrate polymer consisting of D-glucose ($C_6H_{10}O_5$) units joined *via* β-1,4 glycosidic linkages (Fig. 2), with a degree of polymerization (DP) in the range of 1000−30 000 [36,37]. Cellulose in its native state (termed cellulose I) forms crystal structures in the cell walls of plants and trees, whereby polymer chains associate *via* hydrogen bonding to generate bundles of fibrils (also called microfibrillar aggregates, see Fig. 3) [38]. From a morphological point of view, the crystal structures comprise two sub-allomorphs in which highly ordered regions (*i.e.*, crystalline phases) are interspersed with disordered domains (*i.e.*, amorphous phases) in the fibril structure [39]. The presence of amorphous portion varies from species to species, where amorphous domains represent up to 50 % of the structure for some plants while the crystalline regions correspond to approximately 100 % of cellulose generated/extracted from bacteria and some algae [40]. The varying intra- and intermolecular hydrogen-bonding network, as well as the conformations in cellulose, give rise to six interconvertible polymorphs of cellulose (cellulose I, II, III_I, III_{II}, IV_I, IV_{II}), depending on raw material sources and extraction methods [41]. Cellulose I (native state) contains two crystal forms (allomorphs), namely cellulose Iα and Iβ, where Iα is rich in cellulose from algae and bacteria and Iβ is prevalent in tunicates [36]. The distinction between cellulose Iα and Iβ lies in their hydrogen bonding patterns associated with parallel-conformation chains (see Fig. 4); a metastable phase (*i.e.*, Iα) can be converted to the thermodynamically stable phase (*i.e.*, Iβ) *via* high-temperature annealing [42].

2.1.2. Production of cellulose nanocrystals

Notably, a novel form of cellulose, namely cellulose nanomaterials (or nanocellulose), has attracted significant research interest as a prominent and ideal biopolymer in the last two decades, accompanied by the commercialisation of cellulose nanomaterials on a large scale [44]. Generally, the term cellulose nanomaterials describes particles with at least one dimension at the nanoscale (<100 nm) [40]. A few years ago, the Technical Association of the Pulp and Paper Industry (TAPPI) dedicated the standard terms and definition for cellulose nanomaterials (TAPPI WI 3021) based on the nanocellulose size [45]. The nomenclature and abbreviation of various cellulose nanomaterials are illustrated in Fig. 5. More specifically, cellulose nanomaterials can be classified into nano-structured materials and cellulose nanofibres. The first category contains microcrystalline cellulose (MCC) and cellulose microfibrils (CMCs), while the second category consists of cellulose nanofibrils (CNFs) and cellulose nanocrystals (CNCs). Broadly, nanocellulose includes five broad categories based on the cellulose source: CNC (also previously called cellulose nanowhiskers and nanocrystalline cellulose), CNF (also referred to as nano/micro fibrillated cellulose), tunicates-CNCs (t-CNCs), algal cellulose (AC) and bacterial cellulose (BC) [46].

For brevity, two primary types of cellulose nanomaterials extracted

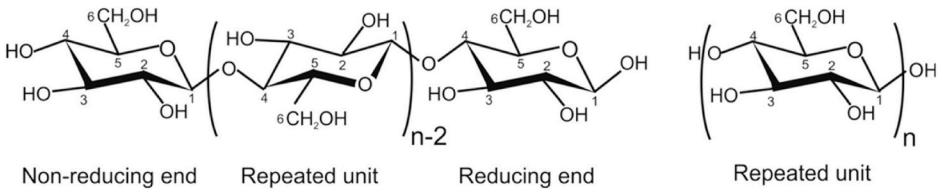

Fig. 2. Chemical structure of cellulose. Reprinted with permission from Ref. [37] (Copyright © 2017, Springer Nature).

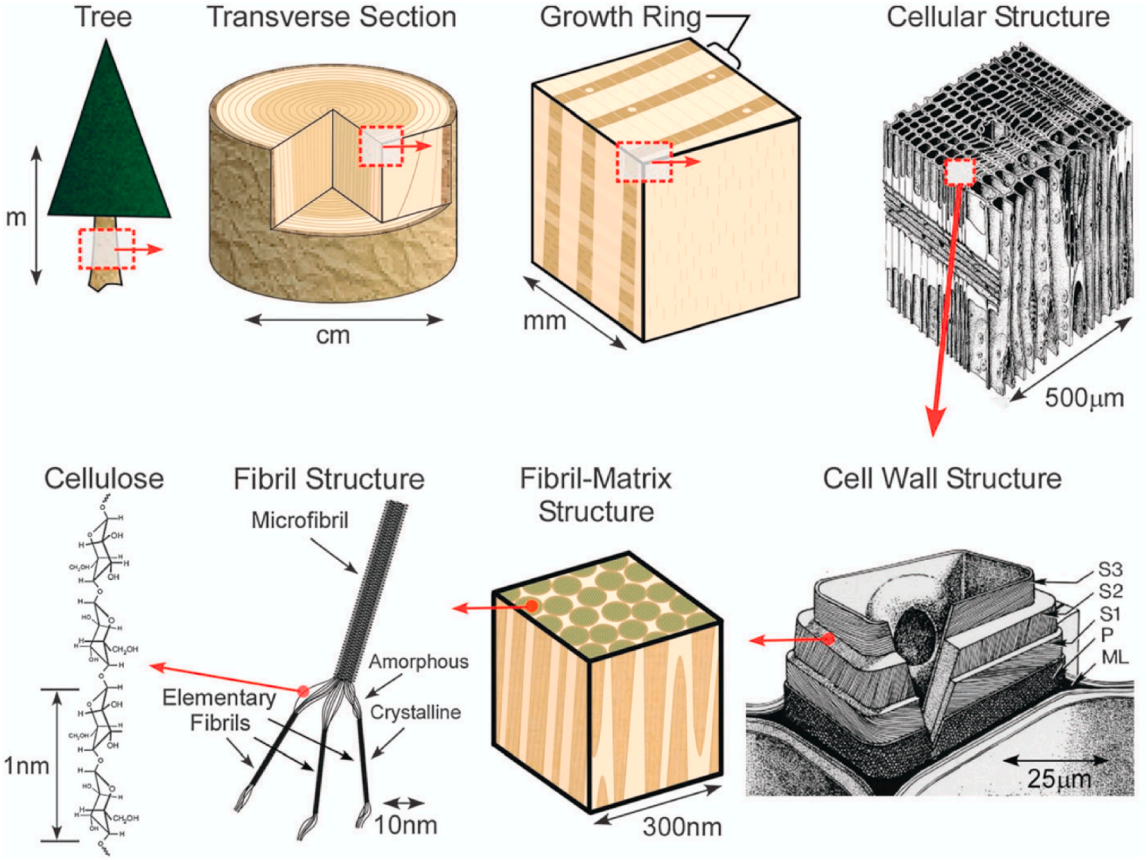

Fig. 3. Schematic illustrating the hierarchical structures of cellulose units in the tree cell wall. Reprinted with permission from Ref. [43] (Copyright © 2010, IOP Publishing).

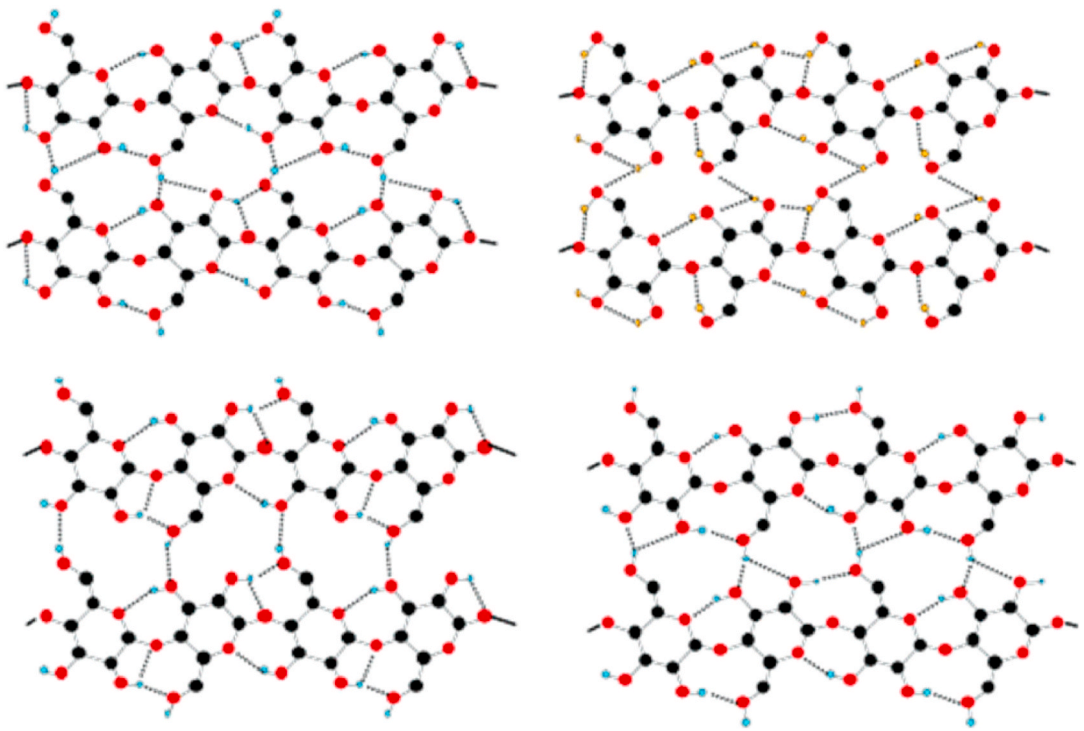

Fig. 4. Hydrogen-bonding networks in cellulose Iα and Iβ. Top: the two various hydrogen-bond patterns in cellulose Iα (left and right); Bottom: the dominated hydrogen-bond network in cellulose Iβ with chains at the origin (left) and centre (right) of the unit cell. C atoms are indicated by black spheres; O atoms are denoted as red spheres and H atoms are indicated by blue spheres. Reprinted with permission from Ref. [41] (Copyright ©2004, American Chemical Society).

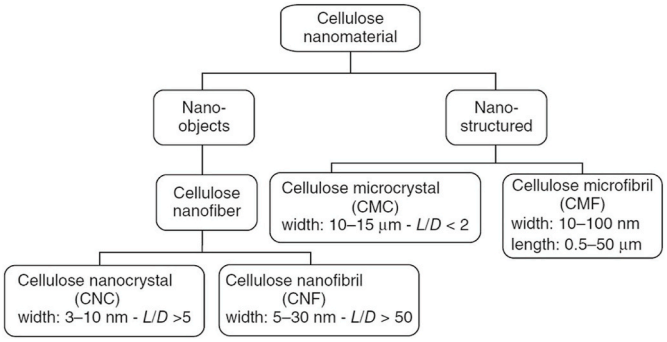

Fig. 5. Standard terms and definition of cellulose nanomaterials (TAPPI WI3021). Reprinted with permission from Ref. [40] (Copyright © 2014, John Wiley & Sons).

from plants, namely CNFs and CNCs, generally comprise pre-treatment steps (*e.g.*, purification and high-pressure homogenisation or microfluidization) and nano-refinement approaches (*e.g.*, mechanical shear or acid hydrolysis) [47]. On the one hand, nano-refinement by mechanical treatments (*e.g.*, cryo-crushing, grinding, high-intensity ultrasonication, or extrusion, *etc.*) under high shear forces to comminute the cellulose materials, resulting in the retainment of particles called CNFs [48]. CNFs exhibit an entangled and flexible network structure, with a fibre/fibril morphology involving long and wide nanofibres (typically 20–100 nm in width; >1 μm in length) with an aspect ratio of 10–100 [49]. On the other hand, nano-refinement by acid hydrolysis (typically sulfuric, hydrochloric, or phosphoric acid) preferentially cleaves the chains in the disordered regions (amorphous regions) of the fibril structure, followed by centrifugation, dialysis, and ultrasonication processes to obtain the remaining crystalline domains, referred to CNCs (see Fig. 6). CNCs are stiff, consisting of rigid, rod-shaped, and highly crystalline nanoparticles with 5–20 nm in width, 50–350 nm in length, and an aspect ratio of 5–30 [50]. In contrast with CNFs, CNCs possess a higher crystallinity (54%–88 %) and superior mechanical properties (*i.e.*, tensile strength of 7.5–7.7 GPa and on-axis tensile modulus of 110–220 GPa) [51,52]. Hence, CNCs are regarded as cost-effective and promising nano-fillers or reinforcements in nanocomposites to replace conventional synthetic polymer composites for the development of various applications. This is attributable to the exceptional reinforcing capability (*i.e.*, high stiffness and mechanical strength) of CNCs (also referred to as crystalline cellulose) among several reinforcement materials (see Table 1) [53].

2.1.3. Applications of cellulose nanocrystals (CNCs)

Notably, CNCs were first produced in 1947 by Nickerson and Harbrle who observed that amorphous regions within the native cellulose

Table 1
Properties of crystalline cellulose and other reinforcement materials. Reprinted with permission from Ref. [53] (Copyright © 2011, Royal Society of Chemistry).

Materials	ρ (g cm^{-3})	σ_f (GPa)	E_A (GPa)	E_T (GPa)
Kevlar-49 fibres	1.4	3.5	124–130	2.5
Carbon fibres	1.8	1.5–5.5	150–500	–
Steel wire	7.8	4.1	210	–
Clay nanoplatelets	–	–	170	–
Carbon nanotubes	–	11–63	270–950	0.8–30
Boron nanowhiskers	–	2–8	250–360	–
CNCs	1.6	7.5–7.7	110–220	10–50

Note.
ρ = density, σ_f = tensile strength, E_A = elastic modulus in the axial direction, E_T = elastic modulus in the transverse direction.

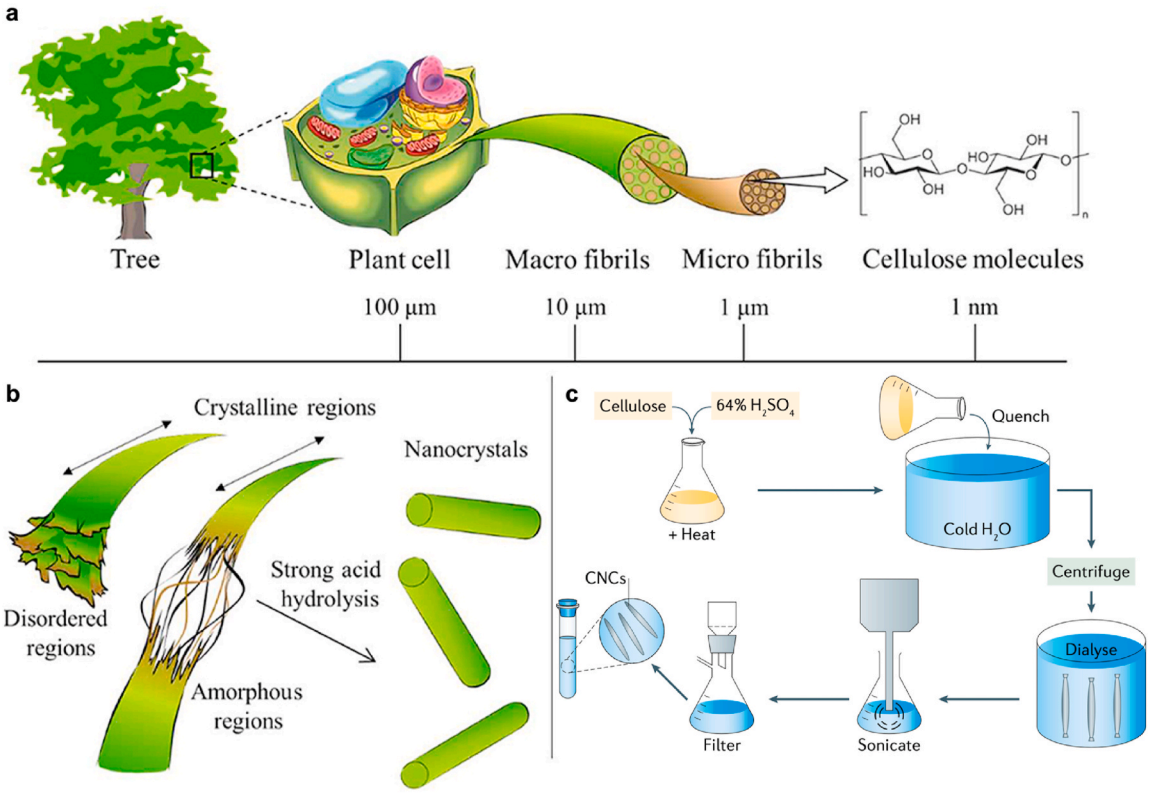

Fig. 6. (a) The hierarchical structure of cellulose in plants or trees from meter to the nanometer scale. (b) Schematic illustrating the strong acid hydrolysis of cellulose to obtain the CNCs. Reproduced with permission from Ref. [54] (CC-BY Open Access, 2020). (c) The laboratory-scale preparation of cellulose nanocrystals (CNCs). Reproduced with permission from Ref. [55] (Copyright ©2020, Springer Nature).

structure were preferentially attacked in the hydrolysis of aqueous hydrochloric or sulfuric acids at boiling temperatures [56]. Inspired by this work, Rånby reported that the colloidal suspensions of cellulose fibres were obtained by controlled sulfuric acid, and cellulose micelles were imaged with electron micrographs in 1949 and 1951, respectively [57,58]. Following these reports, Mukherjee and Woods confirmed the first TEM images of the rod-like single crystallites extracted from different cellulose sources (*i.e.*, ramie hemp, jute, and cotton) [59]. After optimizing the acid-hydrolysis process, Marchessault et al. demonstrated that the presence of rod-like particles stable suspension of cellulose nanocrystallites which can form birefringent gel and liquid crystals alignment [60]. The scientific interest in CNCs has been reignited from the 1990s until now; a timeline illustrating the correlated research and development milestones is displayed in Fig. 7.

Owing to the high tensile strength and modulus, excellent colloidal stability, the tendency to form liquid crystals tendencies and non-toxicity, CNCs have attracted considerable attention as a prominent, sustainable, low-cost nanomaterial that is biodegradable, non-petroleum based, having minimal environmental, animal/human health impact [53,61,62]. In the last two decades, numerous research has focused on developing diverse applications of CNCs and CNC-reinforced nanocomposites (Fig. 8), where CNC-based nanocomposites can be used as one-dimensional (1D) electrospun nanofibres, two-dimensional (2D) membranes, and three-dimensional (3D) aerogels. Their diverse applications range from water purification technologies, biomedical engineering, food and cosmetic modifiers, and energy storage and electronics sectors to construct a desirable carbon-neutral and cost-effective alternative to fossil fuel-based polymers for industrial up-scaling [55,63,64].

2.2. CNC-reinforced nanocomposites

Today, a wide range of polymers have been reported as the matrices for CNC-reinforced nanocomposites, such as poly(vinyl alcohol) (PVA) [65], poly(lactic acid) (PLA) [66], polystyrene (PS) [67], polyurethane (PU) [68], poly(ethylene oxide) (PEO) [69], and polyetherimide (PEI) [70]. This section of the literature review focuses on providing a generalized description of CNC/PEO and CNC/PEI nanocomposites, as described below.

2.2.1. CNC/PEO nanocomposites

PEO is a benign water-soluble polymer compound with a chemical structure of $H-(O-CH_2-CH_2)_n-OH$ with a high molecular weight (>20 000 g/mol) [71]. As a commercially available product, PEO has several advantages such as low cost, low toxicity [72], high safety, easy fabrication, good electrochemical stability and high-temperature stability (up to 150–200 °C) [73], suitable for a variety of applications such as chemical, medical, biological, and electrochemical applications [71]. Specifically, PEO is one of the most commonly used binders for both cathodes and anodes in lithium-ion batteries [74–76], and cathodes in lithium-sulfur batteries [77–79].

Recently, Beard and Eichhorn [80] fabricated highly porous carbon aerogels derived from CNC/PEO in a solvent-free aqueous environment *via* the freeze-drying method of ice gels followed by a carbonisation process at 600 °C, which reduced the environmental effect and improved ease of processing. They used PEO as a binder of CNCs nanoparticles and investigated the effect of the slow and rapid freezing rate on the morphology of CNC/PEO aerogels, exploring how to form tunable pore structures by control of the freezing rate. Xu et al. [81] produced CNC/PEO nanocomposite films by solution casting, showing improvements of 23 %, 44 %, and 512 % in Young's modulus, stress-at-failure, strain-at-failure, respectively, at a CNC content of 7 wt%. As a result, these reported works showed great potential for the use of CNC/PEO as precursors with a solvent-free aqueous synthetic process for carbon aerogels as electrodes applied in low-cost, sustainable energy storage applications.

2.2.2. CNC/PEI nanocomposites

PEI is one of the important classes of high-performance engineering thermoplastics [70], and its chemical structure is shown in Fig. 9. Its aromatic ring structure along the backbone enhances the thermal properties (*i.e.*, decomposition temperature at 510 °C and relative thermal index (RTI) of 170 °C with high long-term heat resistance, mechanical and chemical properties (resistance with most chemicals such as hydrocarbons, halogenated solvents), and dimensional stability (low and uniform coefficient of thermal expansion) [82]. Additionally, its flexible aromatic ether linkages allow good processability which can be easily processed by injection or blow moulding, extrusion, casting, or fibre spinning [83]. Hence, in many structural applications, PEI could substitute metals and other high-performance materials, which have been widely applicable in high-performance applications such as the electronic and electrical industry as well as automotive and aerospace parts [84].

Notably, CNCs are a good choice as a reinforcement of nanocomposites owing to their excellent mechanical properties and structural features, as confirmed by Wang et al. [86] who demonstrated that the CNCs could reinforce PEI electrospun nanofibrous interleaves, leading to increases of 28 % and 20 % respectively in the Mode-I and Mode-II interlaminar fracture toughness of carbon fibre/epoxy composites in comparison to those interleaved with neat PEI nanofibres. Moreover, Chae et al. [70] reported the effect of CNC concentration on the mechanical and structural properties of CNC/PEI nanocomposites fibres *via* a dry-jet wet-spun technique, showing that the incorporation of CNCs with a 5 wt% concentration could improve the tensile modulus of PEI polymer fibres with a 114 % enhancement. They also revealed that the degree of orientation of CNC nanofillers along the fibre axis had a noticeably positive correlation with an increasing draw ratio or mechanical stretching force upon drawing. This accordingly increased the tensile strength and modulus of nanocomposite fibres due to the enhanced long-range order and the stiffening effect of imide rings by hydrogen bonding.

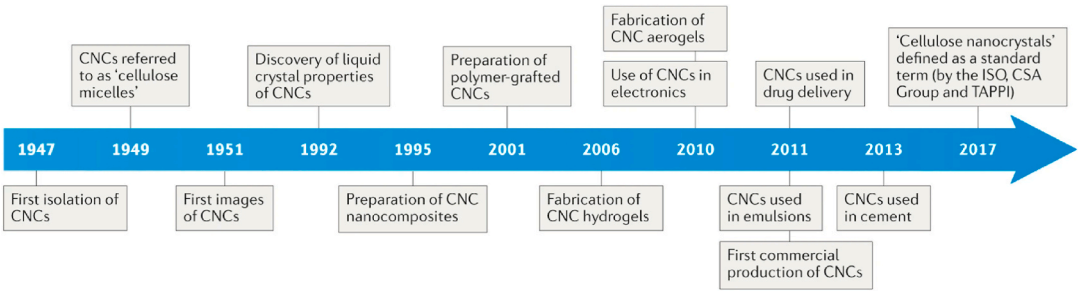

Fig. 7. Research milestones and terminology progress of CNCs in history. Reprinted with permission from Ref. [55] (Copyright © 2020, Springer Nature).

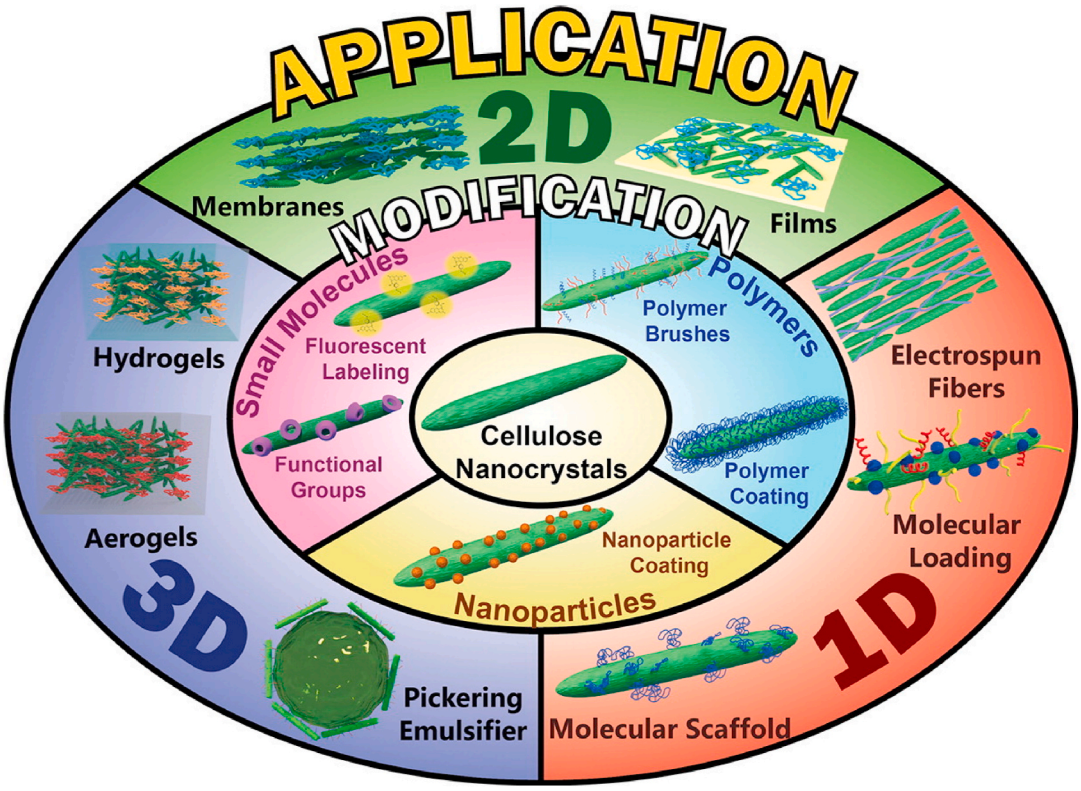

Fig. 8. Schematic illustration of CNCs and CNCs-based nanocomposites applicable in the design of thin electrospun fibres, membranes, and aerogels for various applications. Reprinted with permission from Ref. [63] (Copyright © 2017, Elsevier).

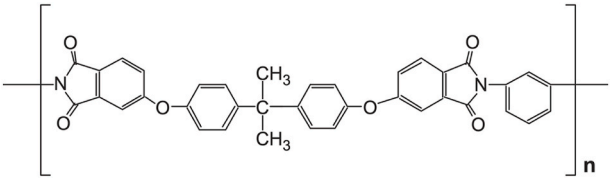

Fig. 9. The chemical structure of polyetherimide (Ultem® 1000). Reprinted with permission from Ref. [85] (Copyright © 2014, Elsevier).

2.3. *Unique strategies or microstructures*

2.3.1. *Ice-templating strategy*

2.3.1.1. Fundamental principles. Ice-templating (*i.e.*, freeze-casting) is one of the most widely utilized and well-tried strategies for fabricating porous materials, enabling the formed pores to a replica of growing ice crystals after sublimation [87]. The first observation of the microstructure formation of gels dependent on the freezing rate can be traced back to 1926 [88], while several elaborate and epoch-making reports have aroused a surge of interest in ice-templating techniques over the last two decades [89–91].

Basically, the ice-templating strategy is a straightforward, low-cost, and scalable assembly technique containing four fundamental processing steps as follows: i) the preparation of a typical suspension or slurry consisting of a solvent (*e.g.*, environmentally-friendly water, *etc.*), solid functional materials and binders; ii) freezing the suspension is the dominating process to determine the resulting architectures and functionalities, which involves multidirectional (isotropic) or unidirectional (anisotropic) freezing approaches [92]. By unidirectionally freezing concentrated suspensions, the suspended particles are expelled from the growing ice crystals fronts and concentrated within aligned channels between the forming ice crystals [89]; iii) the solidified ice crystals are sublimated into a gas *via* lyophilization or freezing-drying at relatively low pressure and temperature to construct porous scaffolds/aerogels; iv) post-treatment for porous scaffolds, such as densification, carbonisation, and infiltration of other components, endowing the final aerogels with enhanced properties [93].

2.3.1.2. Unidirectional ice-templating. The ice-templating strategy is a versatile, low-cost, and scalable assembly technique, allowing control over the pore size and morphology by various types of freezing directions, which can be classified into multidirectional, or unidirectional ice-templating techniques [94]. Multidirectional (*i.e.*, isotropic) ice-templating promotes the randomly formed ice crystals *via* the isotropic freezing-casting throughout the suspension in a standard freezer or immersing the sample into the polystyrene box filled with cooling sources/agents (*e.g.*, liquid nitrogen), resulting in randomly-oriented pores after the sublimation to produce the homogenous, porous aerogels with the nearly isotropic behaviour (see Fig. 10a) [95]. Notably, unidirectional (*i.e.*, anisotropic) ice-templating techniques have been intensively investigated, which are depicted in Fig. 10b. Generally, typical ice-templating equipment comprises three essential components: cooling agents (*e.g.*, liquid nitrogen), a thermally conductive base (*e.g.*, copper rod), and a thermally insulating mould (*e.g.*, Teflon). Unidirectional freezing of the suspensions is achieved by pouring them into the polytetrafluorethylene (Teflon) moulds sitting on a copper cold finger in contact with a liquid-nitrogen bath. The temperature of the 'cold finger' is typically regulated *via* a thermocouple and heat controller to control the velocity of the freezing front. More importantly, the ice crystals thus formed with a preferential growth direction will build uniformly aligned macropores with an anisotropic orientation, and their pore morphology and size directly depend on the particle size in the suspension and the speed of ice solidification [96]. It is noteworthy that the solidification velocity can be influenced by the cooling rate and material concentration, where a reduction in

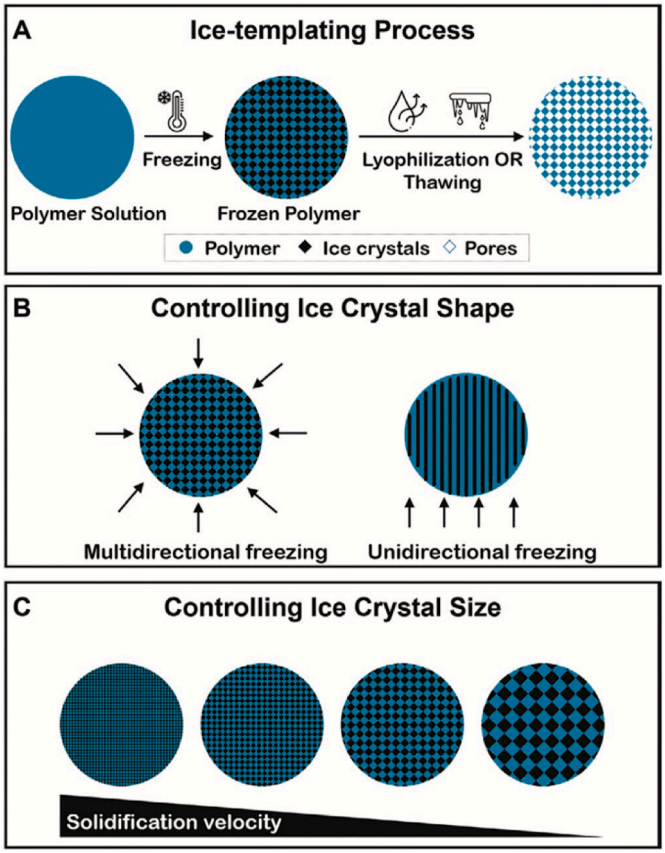

Fig. 10. Schematics illustrating (a) the basic principles of the ice-templating process, (b) the multidirectional or unidirectional freezing method to control ice crystal shape, and (c) the solidification velocity (*i.e.*, cooling rate)-ice crystal size correlations. Reprinted with permission from Ref. [94] (Copyright © 2021, John Wiley and Sons).

solidification velocity results in an increase in the tip radius of an ice crystal and the resulting macropore width (Fig. 10c) [97]. Consequently, by controlling the freezing kinetics or cooling rate of the cold finger, the aerogels with aligned microstructures or anisotropic porosity with the tailored features and necessary physical parameters are obtained.

2.3.1.3. Ice-templated aerogels with aligned microstructures. The unidirectional ice-templating technique offers a versatile and readily accessible approach to fabricating highly anisotropic porous nanocomposite aerogels with aligned microstructures [98]. These aerogels have been researched for a wide range of applications including thermally insulating ceramics [98], filtration or selective biological cell infiltration [90], as well as electrodes of solid-state batteries [99], organic batteries [100], and supercapacitors [101].

Notably, ordered and aligned architectures in advanced aerogels favour simultaneous enhancements in both electrical conductivity and mechanical strength [102]. Recently, Xu et al. [102] also used this technique to report "core-shell" structured graphene aerogel fibres with aligned pores from spinning liquid crystalline graphene oxide (GO) gels. The well-aligned graphene aerogel fibres with interconnected pores offer a high specific tensile strength of 188 kN m kg^{-1}, high compression modulus of 3.3 MPa (the value for graphene aerogels without sheet alignment is 390 kPa), and good electrical conductivity ranging from 2.6×10^3 to 4.9×10^3 S m^{-1}. Renewable and biopolymer-based nanocomposites comprising CNFs or CNCs as nano-reinforcing materials and water-soluble polymer (*e.g.*, PVA or PEO) as a matrix, were extensively used for producing functional, ice-templated and aligned aerogels. Adu et al. [103] used CNFs from paper mill sludge as precursors and poly (vinyl alcohol) (PVA) as a polymeric binder and fabricated CNF/PVA porous foams with a lamellar channel structure *via* the unidirectional ice-templating method, showing a low density of 0.03 g/cm^3 and compressive strength of around 100 kPa at 20 % strain.

Within the last decade, there has been a growing interest in CNC-based composite aerogels due to their enhanced mechanical properties of the resulting nanocomposites [104–106]. Seantier et al. [104] reported that an addition of 10 wt% of CNCs into bleached cellulose fibres aerogels resulted in an increase of up to 377 % in compression modulus compared with neat bleached cellulose fibres (BCF) aerogels. Gawryla et al. [106] utilized CNCs derived from tunicates and montmorillonite clay as reinforcing nanofillers and PVA as a binder to fabricate nanocomposite aerogels *via* a simple freeze-drying method. Interestingly, 2.5 wt% clay and 2.0 wt% CNC nanocomposites aerogels synergistically contributed to a three-dimensional (3D) rigid and porous network, which is consistent with a more than three-fold increase in compressive modulus attributed to the CNCs addition changing from 0.8 wt% to 2.0 wt% with the same concentration of clay (2.5 wt%).

Moreover, Ding et al. [107] demonstrated biomass-derived superelastic carbonaceous nanofibrous aerogels with ordered honeycomb-like and cellular architectures from konjac glucomannan and SiO_2 nanofibres, through a sol-gel electrospinning technique combined with a unidirectional ice-templating and a carbonisation processes. There have been few studies utilizing this unidirectional ice-templating technique for carbonaceous aerogels as electrodes; Schubert et al. [100] reported nonplanar polymer/carbon ice-templated porous electrodes for organic batteries for the first time, which included the fabrication of highly-aligned and pores parallel to the freezing direction at different cooling rates and further investigated the cooling rate-pore diameter relationship (Fig. 11).

2.3.2. Electrospinning strategy

2.3.2.1. Basic concepts. The electrospinning technology was invented by Formhals who produced textile yarns from cellulose acetate in 1934 [108]. Taylor et al. [109] put forward the concept of what has become known as the "Taylor cone" with the shape of the fluid droplet ascribing from electrostatic forces in 1964. The essential components of the electrospinning setup comprise a high-voltage power supply, a syringe pump, a spinneret (basically, a stainless-steel needle with a blunt tip), and a grounded collector [110]. During the typical electrospinning process, a solution is injected into the syringe to produce a droplet as a result of surface tension and then the charged jet is ejected from the spinneret connected to the high-voltage power supply. This ejection occurs because the Taylor cone is formed due to the electrostatic repulsion, which eventually overcomes the surface tension and the stretched fibres are solidified and deposited on the grounded collector such as an aluminium plate or rotating drum (see Fig. 12a) [111]. Specifically, the effects of processing factors (*e.g.*, voltage, viscosity, feed rate, surface tension, *etc.*) on fibre diameter and formation properties *via* an electrospinning method are illustrated in Fig. 13. Some key parameters affect the morphology and diameters of electrospun nanofibres. For instance, the higher electrical conductivity of solvents and increased voltage would cause the finer and smaller nanofibres; conversely, the surface tension and viscosity tend to interfere with the formation of longer and thinner jets from the spinneret, thus the lower surface tension and viscosity would lead to the longer nanofibres with reduced fibre diameters.

In the last few decades, electrospinning's rapid and in-depth development has increasingly attracted attention from the nanostructured fibres or nanomaterials community [113–115]. It is a very simple and effective technique to synthesise one-dimensional (1D) tubular/fibrous nanomaterials with diameters ranging from tens of nanometres to several micrometres. Remarkable progress has been made regarding the applications of electrospun nanofibres or nanofibrous mats, directing

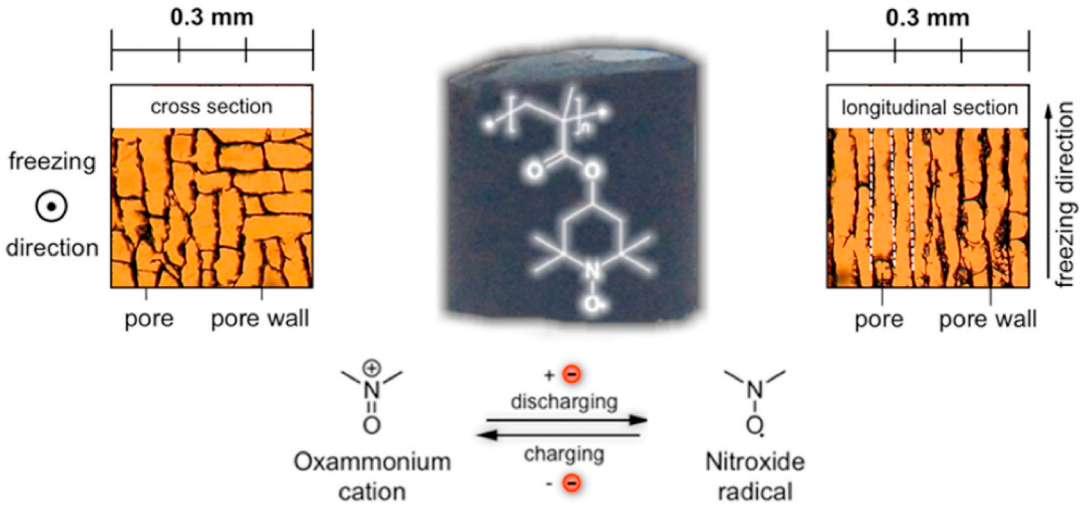

Fig. 11. Ice-templated porous electrodes for organic batteries with aligned pores. Reprinted with permission from Ref. [100] (Copyright © 2016, American Chemical Society).

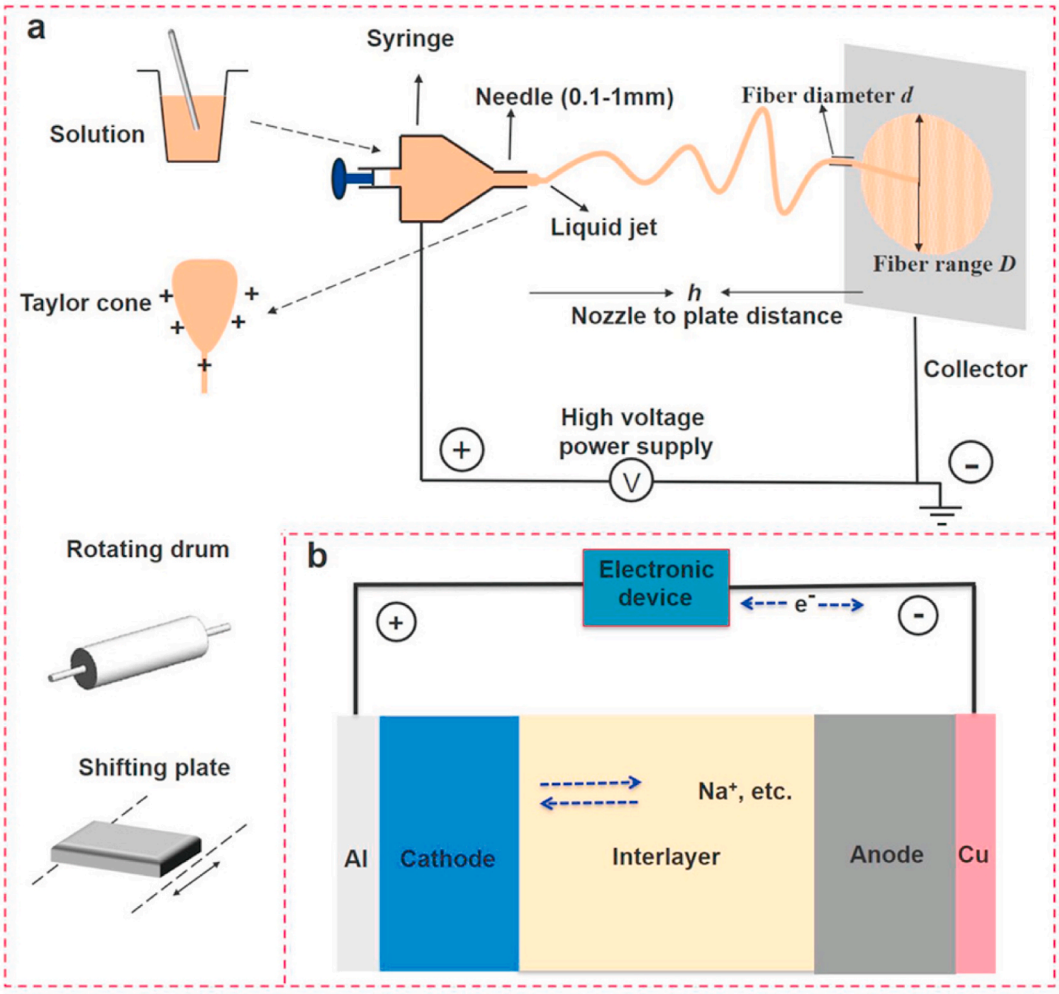

Fig. 12. (a) Schematic illustrations of electrospinning equipment. (b) Schematic configuration of alkali metal ion-based batteries with developing electrospinning strategies to construct essential components (electrodes and separators). Reproduced with permission from Ref. [112] (Copyright © 2020, John Wiley and Sons).

their use towards filtration membranes [116], and biomedical scaffolds (*e.g.*, drug release and biosensing, *etc.*) [117,118], and energy harvesting/conversion/storage constituents (Fig. 12b) [119,120].

2.3.2.2. High-speed electrospinning. To meet the specific requirements of other broader applications, it is also desirable to access the functional/smart electrospun nanofibres with the manipulation of their

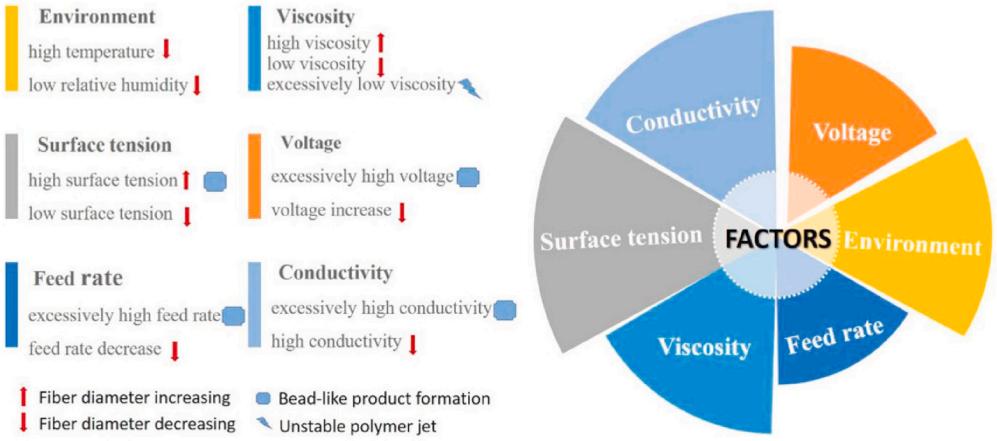

Fig. 13. Parameters influencing the nanofibre formation by electrospinning strategy. Reprinted with permission from Ref. [112] (Copyright © 2020, John Wiley and Sons).

morphologies and alignment [119]. Generally, when the conductive collector is an aluminium plate, electrospun nanofibres with no orientation are fabricated in the form of a nonwoven nanofibrous mat. Alternatively, when using a rotating drum as the collector, nanofibres with a controlled degree of alignment *via* regulating its rotational speed are fabricated (see Fig. 14). By collecting electrospun nanofibres on a high-speed rotating drum, the nanofibres orient along the rotational direction of the drum owing to the mechanical stretching and electrostatic forces [121].

Importantly, compared to randomly oriented nanofibrous membranes with low mechanical and electrical properties obtained *via* the conventional setup, the highly-ordered nanofibres with uniaxially aligned arrays possess increased biocompatibility, mechanical and electrical properties. Recent research has been developed to explore the feasibility of aligned electrospun nanofibres, and some breakthroughs have been accomplished to broaden their prospects as applications in the fields of composites, optoelectronic devices, electrochemical sensors, and many more [123–125].

Daelemans et al. [126] obtained the aligned nanofibrous veils with a preferential orientation by using a rapidly rotating drum at a speed of 4000 rpm and studied their orientation and the effect on the toughening for electrospun nanofibrous veils on the toughening effect for the nanofibre interleaved laminates. Besides, Fennessey et al. [123] reported on highly aligned electrospun polyacrylonitrile (PAN) nanofibres with improved strength and modulus at high rotating speeds of the rotating drum; these high speeds were shown to increase in the molecular orientation determined by dichroism measurements and wide-angle X-ray diffraction patterns. It is noted that previous studies have also demonstrated that the electrospinning strategy with strong stretching forces may generate a preferred orientation of polymer chains along the axis of the aligned fibres [127]. Furthermore, Xu et al. produced aligned single-wall carbon nanotubes (SWCNTs)/PAN nanofibrous membranes, indicating that their alignment could enhance their permeability and wetting properties, which suggests the great potential of these aligned composites membranes as battery separators or electrodes [125].

2.4. *Sodium/potassium-ion batteries*

With the ever-increasing demands for the wide implementation of renewable and intermittent energy sources (*e.g.*, solar and wind), the development of low-cost, sustainable, and large-scale energy storage technologies has become one of the most significant challenges for achieving net-zero emissions energy systems in the future [128]. As highly prospective alternatives to expensive LIBs (Li: 20 ppm in the Earth's crust), sodium-ion batteries (SIBs) and potassium-ion batteries (PIBs) have aroused growing attention in the energy storage field, considering their low cost, natural abundant resources (Na: 23 000 ppm and K: 17 000 ppm in the Earth's crust) and the similar rocking-chair mechanism with LIBs [129–131]. It is worth noting that the performance of SIBs/PIBs lies in the development of electrode materials, hence

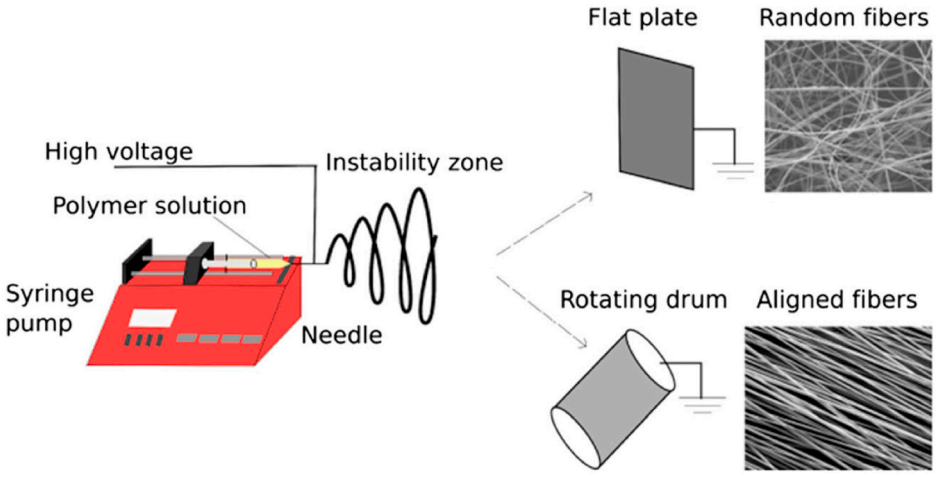

Fig. 14. Schematics illustrating (a) electrospinning setup to produce random nanofibres collected at a flat plate, and (b) to generate aligned nanofibres collected on a rotating drum. Reprinted with permission from Ref. [122] (Copyright © 2016, Springer Nature).

early studies as well as the current work have concentrated on the advances associated with the development of appropriate anode and cathode materials for both SIBs and PIBs [132–134]. This section reviews the literature regarding anode and cathode materials, showcasing typical examples of advanced anode and cathode materials for both SIBs/PIBs.

2.4.1. Anode materials

Graphite, as the common anode material for LIBs, is not satisfactory with SIBs/PIBs due to the energetically unstable Na-C binary intercalation compounds [135]. Therefore, the development of high-performance and suitable anode materials for SIBs/PIBs is highly desired and urgently required. Recent research on the anode materials for SIBs/PIBs has been developed in three key categories according to various reaction mechanisms: (i) the insertion-type; (ii) the alloying-type; and (iii) the conversion-type anodes [136].

2.4.1.1. Insertion-type anode materials. Based on the insertion reaction mechanism during sodiation/desodiation processes, carbonaceous materials and titanium-based oxides are regarded as insertion-type anode materials for SIBs/PIBs [137]. Carbonaceous materials that take the leading position in an anode material's map due to their low cost and commercial potential are classified into graphitic and non-graphitic carbon. Specifically, Wen et al. [138] reported appropriately expanded graphite with an enlarged interlayer spacing of 4.3 Å, exhibiting a reversible capacity of 284 mAh g^{-1} at a current density of 20 mA g^{-1}. Non-graphitic or disordered carbons, including soft carbon (SC) and hard carbon (HC), are attracting more interest as anode materials for SIBs and PIBs because of their relatively larger interlayer spacing in comparison with that of graphite (3.35 Å). SC, which can be graphitised *via* heat-treatment temperature over 2200 °C, was first reported by Doeff et al. [139]. They reported the Na-insertion mechanism of SC anodes obtained by the pyrolysis of Conoco petroleum coke. Stevens and Dahn [140] proposed a "house of cards" storage mechanism of glucose-derived hard carbon, containing the insertion of Na^+ ions between graphitic ordered domains in the sloping region and Na-ions filling of nanopores in the plateau region (see Fig. 15) [141]. Several chemical and structural modifications of carbonaceous materials have been researched to enhance the electrochemical properties, including expanded interlayer spacing, porosity, heteroatom-doping, and various morphologies [142].

Moreover, other biomass-based materials such as cellulose nanomaterials (*e.g.*, CNCs, CNFs, *etc.*) have also been extensively investigated in energy storage applications (Fig. 16). Hu et al. [143] studied CNC-derived porous carbon nanofibres with a large domain of ordered lattice as anodes for SIBs that deliver a high reversible capacity of 340 mAh g^{-1} at a current density of 100 mA g^{-1}. Moreover, Feng et al. [144] coated the cellulose/lignin-derived carbon aerogels on the VSe_2 nanosheets as anodes for PIBs and demonstrated improved long-term cycling stability over 1000 cycles. Recently, Wang et al. [145] innovatively used a unique self-built instrument platform and developed a nature-inspired unidirectional ice-templating method, which can simultaneously adjust the cooling rate (3, 5 and 7 K min^{-1}), orientation, and microstructural features of carbon aerogels from renewable resources as anode materials to tailor the best electrochemical performances of anodes for SIBs/PIBs. This reported work provides new insights into understanding structure-performance correlations regulated by the cooling rates of an ice-templating strategy and design guidelines for electrodes applicable in multiple energy storage technologies (*e.g.*, zinc-, calcium-, aluminum- and magnesium-ion batteries [146], *etc.*). Consequently, biomass-derived hard carbons are attractive and promising for SIBs/PIBs due to their excellent capacity and satisfactory cycling performance.

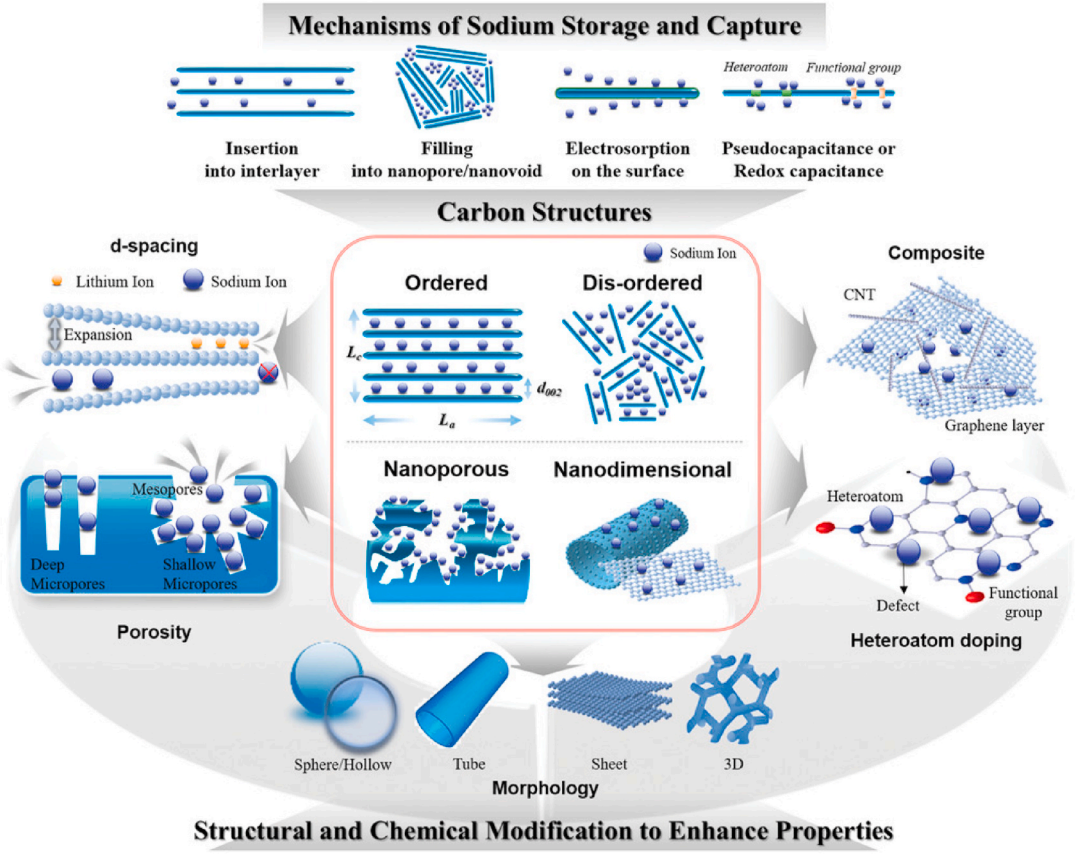

Fig. 15. Schematics illustrating the Na-ion storage mechanisms in carbonaceous materials and strategies to enhance electrochemical properties. Reprinted with permission from Ref. [142] (Copyright © 2019, John Wiley and Sons).

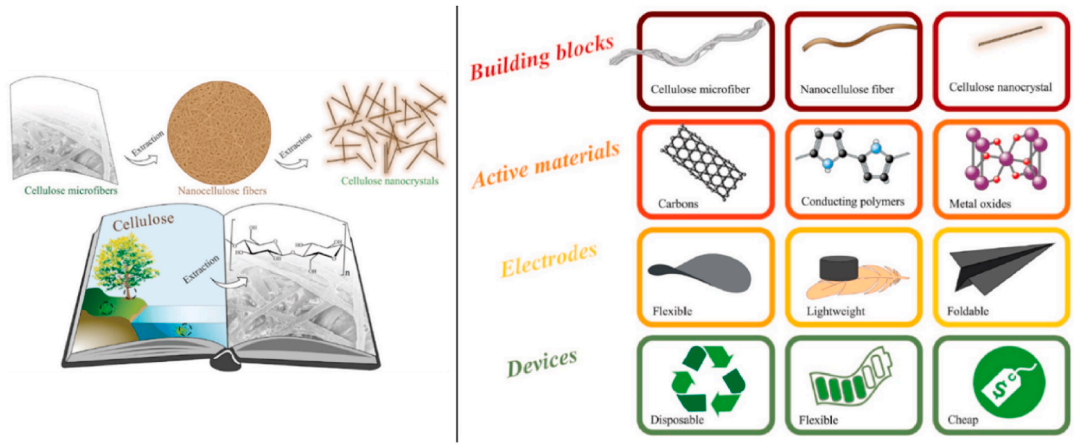

Fig. 16. Schematic illustration of the cellulose building blocks (CMFs, CNFs, CNCs) and cellulose-derived materials and their applications on electrodes and supercapacitors. Reproduced with permission from Ref. [147] (Copyright © 2017, John Wiley and Sons).

Referring to the titanium-based oxides as anode materials, Hu et al. [148] synthesized nanosized $Na_2Ti_3O_7$ as a prospective anode by a solid-state reaction at 1000 °C, systematically investigating the Na-ion insertion/extraction behaviour with a direct transfer pathway ($Na_2Ti_3O_7 \leftrightarrows Na_4Ti_3O_7$). However, the $Na_2Ti_3O_7$ electrode was introduced with serious deficiencies in Coulombic efficiency and capacity retention. Further, Li et al. [149] prepared $Na_2Ti_7O_{15}$ nanotubes on the titanium net substrate as an anode material for SIBs, which showed a large reversible capacity of 258 mAh g^{-1} at a current density of 50 mA g^{-1} and good rate capability of 108 mAh g^{-1} at 1.5 A g^{-1}. This could be ascribed to the 3D network of the Ti substrate and nanoscale wall thickness of $Na_2Ti_7O_{15}$ nanotubes for facilitating the electrolyte percolation and shortening the pathway of Na-ion transport.

2.4.1.2. Alloying-type anode materials. Alloying materials have attracted much attention in the pursuit of high-energy-density anodes for SIBs/PIBs because of the multiple electron transfer during the alloying/dealloying reactions [150]. Metals (*e.g.*, Sn, Bi), metalloids (*e.g.*, Sb, Si, Ge) and phosphorus (P) have been extensively investigated as potential anodes for SIBs/PIBs. For example, metallic tin (Sn) can alloy 3.75 Na^+ per Sn atom and deliver a high theoretical capacity of 847 mAh g^{-1} [151]. Wang et al. [152] fabricated Sn core-shell nanorods (C/Sn/Ni/TMV1cys) with vertical alignment as anodes *via* a self-assembly strategy on stainless steel (Fig. 17). They reported that the resultant Sn nanorod delivered a high capacity of 722 mAh g^{-1} in the initial cycle with a capacity retention of 56 % after 150 cycles for SIBs (see Fig. 17b). The unique vertical alignment can mechanically accommodate >500 % volume change during sodiation/desodiation processes.

Furthermore, germanium (Ge) can only uptake one Na atom and Na-Ge compounds can deliver a theoretical capacity of 369 mAh g^{-1} [153]. Mitlin et al. [154] demonstrated a high capacity of 360 mAh g^{-1} at 1C and 310 mAh g^{-1} at 4.0C for the lithiated Ge thin films as anodes of SIBs, signifying the enhanced rate capability due to the introduction of denser nanopores *via* the Li activation at 0.1C. Notably, metallic P provides the highest theoretical capacity of 2596 mAh g^{-1} which is derived from the formation of Na_3P alloy among present SIB anodes [155]. Cui et al. [156] fabricated a sandwiched graphene-P-graphene hybrid anode material that exhibits an ultrahigh specific capacity of 2440 mAh g^{-1} at 50 mA g^{-1} with a dual intercalation-alloying mechanism. The graphene layer plays a role of a mechanical backbone to buffer the volume expansion along the *z*-axial direction during cycling operation.

2.4.1.3. Conversion-type anode materials. Transition metal compounds (M_aX_b, M = transition metal, X = O, S, P, N, F, *etc.*) have been studied as potential anode materials for SIBs/PIBs to adopt Na^+ by conversion reactions [157]. Generally, great interest and efforts were devoted to researching transition metal oxides such as iron oxides [158], copper oxides [159], and cobalt oxides [160]. Particularly, iron oxides (*e.g.*, Fe_2O_3, Fe_3O_4, *etc.*) offer a high theoretical capacity of ~1000 mAh g^{-1}. Recently, Zhou et al. [161] embedded Fe_3O_4 quantum dots in 3D carbon by utilizing an *in-situ* quantization technique and a template of a metal-organic framework (MOF) as anodes for ultrafast rechargeable SIBs with battery-like capacities and capacitor-like rate capabilities.

Li et al. [128] designed $CoSe_2$-$MoSe_2$/reduced graphene oxide (rGO) tubes with a hierarchical structure *via* hydrothermal and selenization treatments. They reported that the $CoSe_2$-$MoSe_2$/rGO tube exhibited a

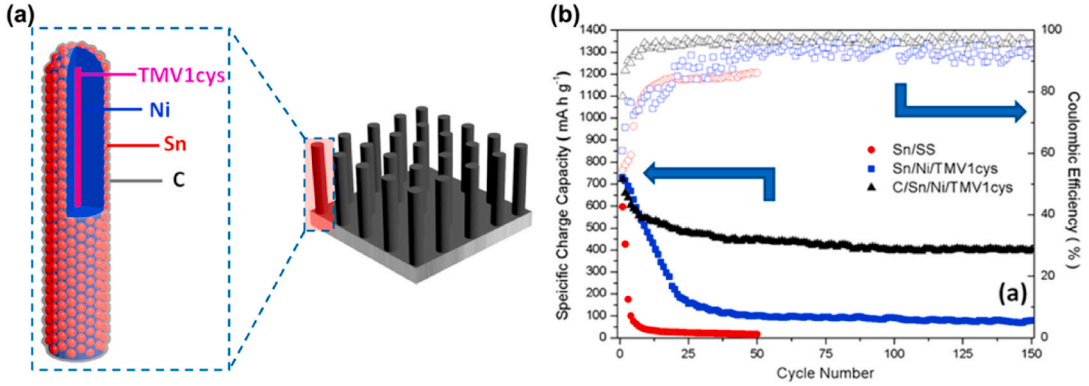

Fig. 17. (a) Schematic illustration of the 3D Sn/Ni/TMV1cys anode. (b) Cycling stability of Sn thin film, 3D Sn/Ni/TMV1cys and C/Sn/Ni/TMV1cys anodes. Reprinted with permission from Ref. [152] (Copyright © 2013, American Chemical Society).

capacity of 584 mAh g^{-1} at 0.1 A $g^{-1}$and 393 mAh g^{-1} at 5 A g^{-1} as anodes of PIBs with an intercalation-conversion mechanism, respectively. Transition metal sulphides represent promising conversion-type anode materials for SIBs because of the better reversibility of Na_2S than Na_2O during the sodiation-desodiation process. Kang et al. [161] synthesized tin sulphide (SnS) 3D flowers with a hierarchical nanosheet that showed an initial capacity of 400 mAh g^{-1} involving the conversion-alloying reactions ($SnS + 2Na^+ + 2e^- \leftrightarrow Na_2S + Sn$; $4Sn + 15\ Na^+ + 15e^- \leftrightarrow Na_{15}Sn_4$).

2.4.2. Cathode materials

A broad range of compounds, including layered oxides, polyanionic compounds, Prussian blue analogues, and organic compounds based on the intercalation reaction have been studied as potential cathode materials for SIBs/PIBs (see Fig. 18e) [136].

Layered oxides. A_xTMO_2 layered oxides ($0 < x < 1$; A = alkali metal, TM = transition metal) are classified into four groups (*i.e.*, P2-, O2-, O3-, P3-type) based on the packing number of Na^+/K^+ prismatic ("P") or octahedral ("O") layers and the stacking sequence of Na^+/K^+ between layers (Fig. 18a), where the nucleation of O2 phase in P2 crystallite can exist in several parts of crystals with the two gliding vectors, (2/3, 1/3, 0) and (1/3, 2/3, 0) [166]. Na_xTMO_2 layered oxides are one of the most promising families of cathode materials for SIBs/SMBs but still face three major challenges, such as irreversible phase transition, air instability and insufficient battery performance [167]. Luo et al. [168] reported layered P2/P3-type K_xMnO_2 (x = 0.3 and 0.45) cathodes *via* a co-precipitation approach for PIBs, while $K_{0.45}MnO_2$ exhibits a smaller particle diameter, a higher reversible capacity of 129 mAh g^{-1} at 20 mA g^{-1} and better rate performance of 51 mAh g^{-1} at 200 mA g^{-1} in comparison with those for $K_{0.3}MnO_2$.

Polyanionic compounds. Polyanionic compounds have been highlighted as high-voltage cathode materials by several researchers for high-capacity SIBs/PIBs [169]. Polyanionic compounds (*e.g.*, $Na_3V_2(PO_4)_3$, $Na_3(VO_x)_2(PO_4)F_{3-2x}$ ($x = 0$ or 1), *etc.*) are apparently a common cathode due to their high working potential, while the use of the toxic and expensive vanadium element remains a critical issue in real applications [170]. Particularly, $Na_3V_2(PO_4)_3$ (NVP, Fig. 18b) with a NASICON-type (Na superionic conductor) structure shows a long-term cyclability and high Na^+ diffusion rate. For instance, Hu et al. [171] found two various Na sites (M1, M2) with co-existent different coordination, where the extraction of Na^+ only locally occurs at M2 sites and M1 sites remain immobilised.

Prussian blue analogues. Prussian blue analogues (PBAs, see Fig. 18c) with the general formula ($A_xM_1M_2(CN)_6$) (A = alkali, M_1, M_2 = Mn, Fe, Co, Ni) are the most widely investigated cathodes in both aqueous and non-aqueous SIBs/PIBs, while their interstitial water is difficult to be removed and affects the cell performance [172]. Specifically, $Na_xMFe(CN)_6$ has been the suitable choice due to its nontoxicity and low cost. Goodenough et al. [173] reported the $Na_2MnFe(CN)_6$ framework with the removal of interstitial H_2O, and the dehydrated $Na_2MnFe(CN)_6$ delivered a superior reversible capacity of 150 mAh g^{-1} at a flat plateau at 3.5 V with excellent cycling stability with a 75 % capacity retention over 500 cycles.

Organic Compounds. On the other hand, organic compounds (*e.g.*, organic acid anhydride, see Fig. 18d) have also attracted attention as cathodes for SIBs/PIBs due to their renewability, lower cost and better safety features [174]. Meanwhile, a well-known organic pigment, 3,4,9, 10-perylenetetracarboxylic dianhydride (PTCDA) was reported to be chemically stable during the charge/discharge process). Additionally, as one of the important precursors in the dye industry, the mass production of PTCDA offers the possibility to be widely used as a low-cost cathode material for SMBs [175,176]. Ji et al. [174] demonstrated that PTCDA itself displayed a capacity of 145 mAh g^{-1} at 10 mA g^{-1} and a good rate capability of 91 mAh g^{-1} at 1 A g^{-1} in a potential range of 1−3V,

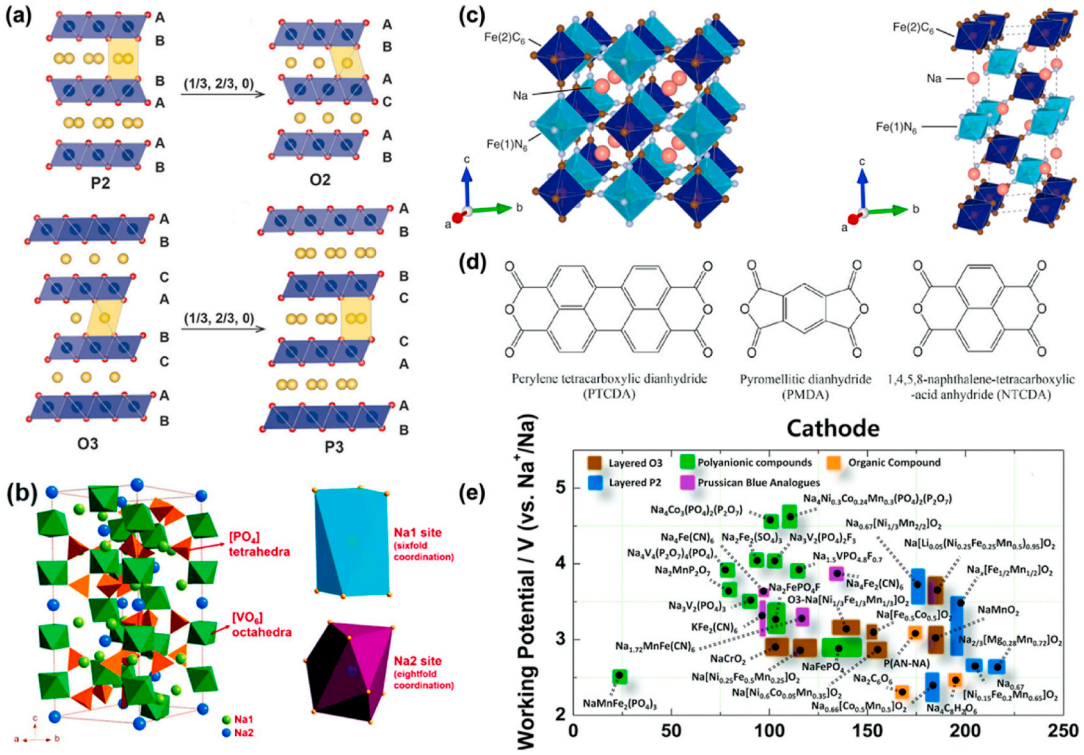

Fig. 18. Presentative crystal structures of (a) layered oxides (P2-, O2-, O3-, P3-type). P2-type Na_xTMO_2 comprises two kinds of TMO_2 layers (*i.e.*, AB and BA). Reproduced with permission from Ref. [162] (Copyright © 2017, John Wiley and Sons). (b) Polyanionic compound (rhombohedral ($Na_3V_2(PO_4)_3$). Reproduced with permission from Ref. [163] (Copyright © 2009, RSC Pub). (c) Prussian blue. Reproduced with permission from Ref. [164] (Copyright © 2020, Springer Nature). (d) Selected organic compounds. Reproduced with permission from Ref. [165] (Copyright © 2020, John Wiley and Sons). (e) Recent research progress in cathode materials for SIBs. Reproduced with permission from Ref. [136] (Copyright © 2017, The Royal Society of Chemistry).

illustrating the reduction of two carbonyl groups to form Na_2PTCDA (see Fig. 19).

Given that cathode materials are the key component that determines the energy and cost of batteries, it is necessary to discover or deploy more low-cost suitable cathode materials to satisfy their overall renewability/sustainability. This choice has to consider the economic and environmentally-friendly benefits for the potential commercialisation and practical applications of SMBs in the future.

2.5. Sodium-metal batteries

Recently, research interests have focused on the Na metal as anode materials for the next-generation rechargeable batteries due to its high theoretical specific capacity (1165 mAh g^{-1}), low redox potential (−2.71 V vs. SHE) and abundant resources [177]. High-energy-density sodium-metal batteries (SMBs) with Na metal anodes and cathodes (*e.g.*, high-voltage cathodes, room-temperature (RT) Na-S, Na-O2, Na-$CuCl_2$, *etc.*) are competitive alternatives to the current state-of-the-art LIBs [178]. However, there are still several challenges to be overcome for practical applications of rechargeable SMBs.

2.5.1. Mechanisms and challenges

It is well known that a typical battery consists of four essential components: anode, cathode, electrolyte, and separator. During charging, Na ions are extracted from the cathode and plated on the surface of the Na metal anode to gain the electrons *via* a redox reaction, thus re-forming the Na atoms; while the Na metal is stripped from the anode to insert onto the cathode upon discharging [179]. Owing to its high chemical reactivity and low mechanical properties [180], most organic electrolytes can be reduced at the Na metal surface to generate the solid electrolyte interphase (SEI). During the plating/stripping process, the Na anode undergoes large volume expansion/contraction, thus inducing the breakage of the SEI layer to accelerate the nonuniform Na plating and Na^+ flux, which causes the dendrites growth surrounding the cracks/tips during further Na plating. During the subsequent stripping process, the Na dendrites are detached from the vulnerable root of the anode bulk to construct the "dead" Na [181]. After repeated plating/stripping behaviour of Na^+/Na, the accumulation of "dead" Na and the growing dendrites would penetrate through the separator, finally leading to the internal short circuit of the battery [182]. The schematic illustration for the Na dendrite formation is displayed in Fig. 20. Therefore, the major impediments to the development of SMBs are associated with uncontrolled dendrite growth, degradation of battery cycle life, and an ultimate short-circuit when Na dendrites penetrate the separator to reach the cathode, posing serious safety concerns [183].

2.5.2. Optimization strategies

To address the aforementioned issues, various strategies that have been previously employed for lithium metal batteries have also been developed for stabilizing SMBs. Based on the visualized statistics of the top 50 keywords in publications associated with "SMBs" and indexed by the Web of Science since 1900 (Fig. 21), it could be seen that the "performance" of SMBs attracts the greatest attention from researchers. According to the strong links with the "performance" keyword, the formulation and optimization of "anode", "cathode" and "electrolyte" systems currently become research hotspots and the dominant direction by numerous researchers, where the research on separators remain extensively neglected in the field of SMBs. Herein, this section highlights several strategies to suppress Na dendrites growth and improve the performance for achieving stable and highly safe SMBs.

2.5.2.1. Electrolyte formulation. Liquid electrolytes including ester-based electrolytes such as ethylene carbonate (EC), dimethyl carbonate (DMC), and diethyl carbonate (DEC) as well as ether-based electrolytes such as diglyme, dimethoxyethane (DME), and tetraglyme, are widely utilized in the SMBs [184]. Generally, the formulation of solvents, salts and additives is significant in affecting the components of the formed SEI layer and for controlling the reactions between the liquid electrolytes and the Na anode, which in turn influence the electrochemical properties of SMBs.

Ether-based electrolytes. Carbonates-based electrolytes are a commonly used and low-cost choice for research on state-of-the-art and commercial-available LIBs, owing to their higher reduction potentials and better oxidation stability coupled with high-voltage cathodes [185]. Nevertheless, the Na anode shows limited reversible plating/stripping in carbonate-based electrolytes in contrast with ether-based electrolytes [186]. Cui et al. [187] evaluated the reversibility of Na plating/stripping in a series of electrolytes (*i.e.*, various solvents and salts) and found high average Coulombic efficiencies (CEs) of 99.9 % over 300 cycles using the 1 M sodium hexafluorophosphate ($NaPF_6$) in diglyme, monoglyme, or tetraglyme as the electrolyte. Moreover, uniform and nondendritic morphologies were achieved in these cases. While for 1 M $NaPF_6$ in EC/DMC and EC/DEC, very low CEs of ~25 % and nonuniform dendritic deposition morphologies were observed.

Depth-profiling of the SEI layers in these various electrolytes *via* X-ray photoelectron spectroscopy (XPS), it revealed that the formed uniform SEI layer using $NaPF_6$ in diglyme consisted of the inorganic Na_2O and NaF, which was highly impermeable to the electrolyte solvent to facilitate the dendrite-free deposition. However, a thicker SEI layer formed in carbonate solvents was composed of more porous organic components that are prone to the permeability of electrolyte solvents with more side reactions.

High-concentration electrolytes (HCE). The increased concentration of the liquid electrolytes could prolong the Sand's time (*i.e.*, *t*, the time when the ionic concentration of the anode approaches zero or the time close to the appearance of dendrites in the high current-density regime) [188] and defer the onset of the growth of dendrites accordingly (*t* is dependent on the concentration *C*) [189]. Choi et al. [190] proposed ultraconcentrated electrolytes composed of 5 M bis(fluorosulfonyl)imide (NaFSI) in DME, exhibiting a high CE of 99.3 % over 120 cycles of Na plating/stripping. They elucidated that the contribution could be ascribed to the participation of the solvation structure

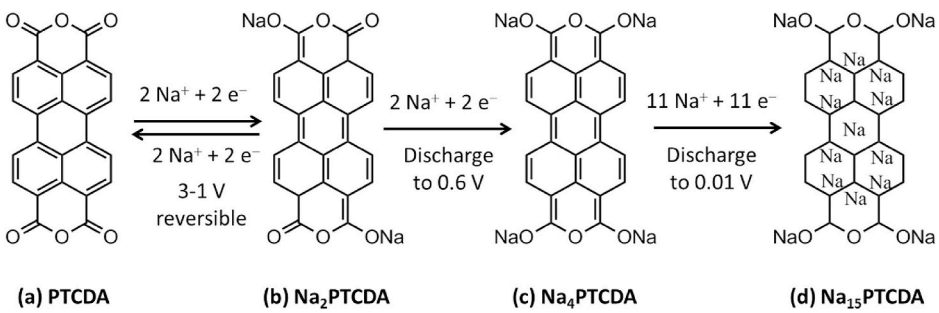

Fig. 19. Schematic diagrams for the proposed electrochemical reactions during sodiation/desodiation of PTCDA. Reprinted with permission from Ref. [174] (Copyright © 2014, John Wiley and Sons).

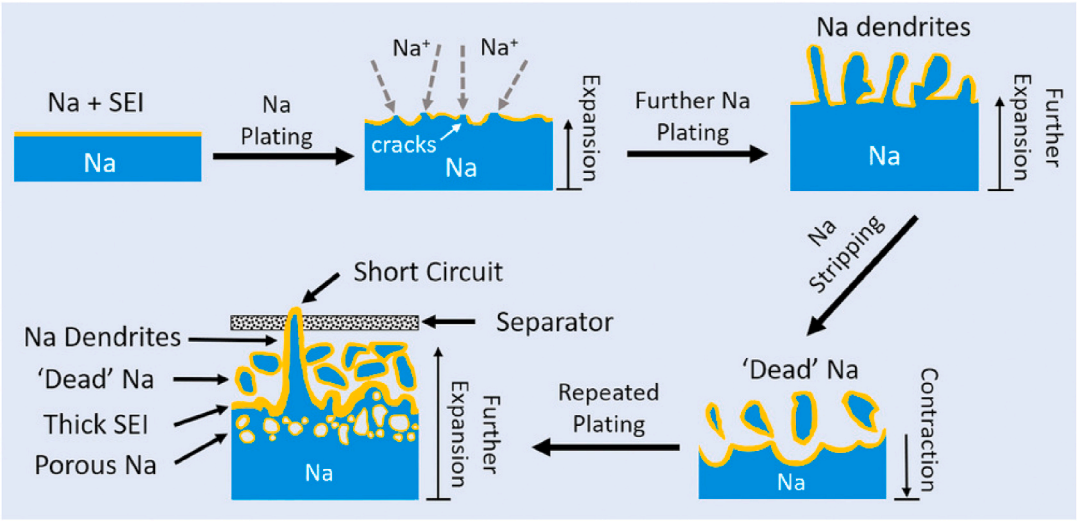

Fig. 20. Schematic illustrating the stripping/plating behaviour of Na^+ and the formation process of Na dendrites. Reprinted with permission from Ref. [182] (Copyright © 2019, John Wiley and Sons).

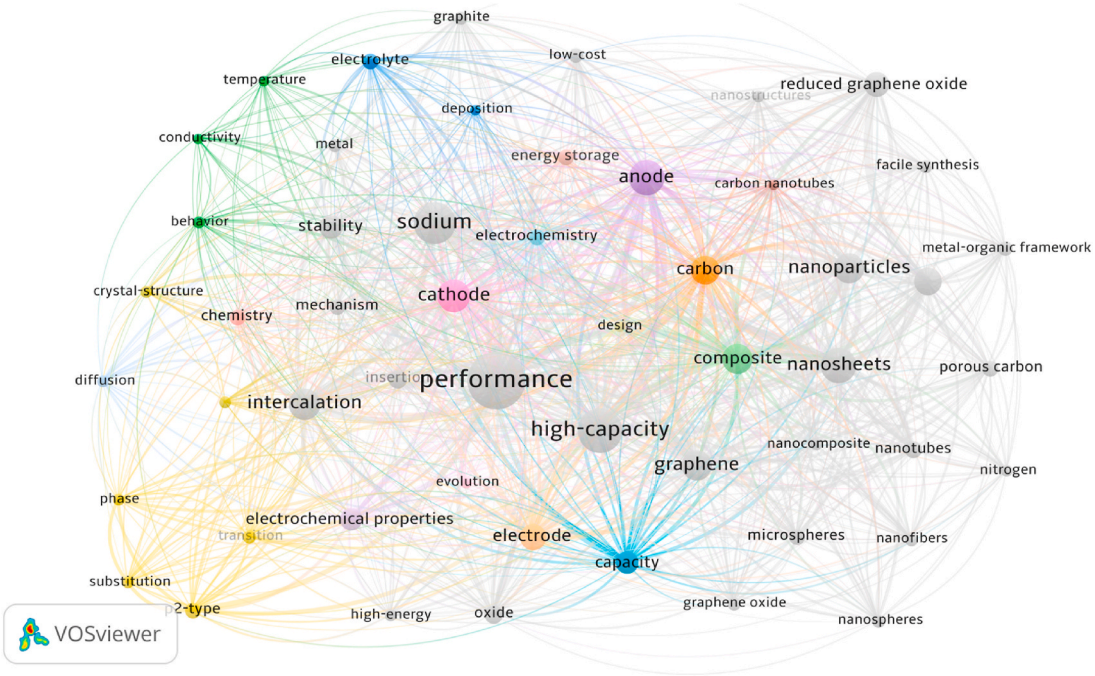

Fig. 21. The visualized statistics of keywords in publications related to sodium metal batteries since 1900 indexed by Web of Science, where the colour represents the average publication year, and the size indicates the reported frequency in the literature.

$(Na^+(DME)_{1-x}(FSI^-)_x)$, which decreases the number of free solvent molecules to alleviate the relevant side reactions, especially at > 2 M NaFSI. However, the costly price of high-concentration salt and poor wettability associated with the high viscosity would present new challenges for large-scale applications of SMBs.

Electrolyte additives. Fluorinated compounds such as fluoroethylene carbonate (FEC) have been investigated as electrolyte additives by modulating the properties of the SEI layer in anode research on SMBs [191,192]. The highest occupied molecular orbital (HOMO)-lowest unoccupied molecular orbital (LUMO) energy-level diagram (Fig. 22), where The HOMO-LUMO energy-level diagram revealed that FEC has a relatively low LUMO energy level and a higher electron affinity compared with those of conventional carbonates [193]. Conventional carbonates tend to generate unstable interlayers with undesirable decomposition, while DME is highly oxidative with high-voltage cathodes due to its high HOMO energy level. Accordingly, the interlayer formed *via* the reductive decomposition of FEC molecules blocks further decomposition reactions between the solvents with the Na metal anode [194]. Recently, Choi et al. [193] added an FEC additive into the 1 M NaFSI in polycarbonate (PC)/EC (v/v, 1:1) electrolyte, which demonstrated the construction of a mechanically strong NaF-containing SEI layer with enhanced ion-permeability to suppress its breakage and induce a homogenous Na deposition. They reported that a high CE of ≈94 % was attained in FEC-based electrolytes over 100 cycles with the reversible plating/stripping of the Na metal anode. Unfortunately, F-based electrolytes (*e.g.*, $NaPF_6$, NaFSI, FEC, *etc.*) show several drawbacks such as the environmental unfriendliness and harmful formation of HF, decomposition at high temperatures, and water ingress impeding

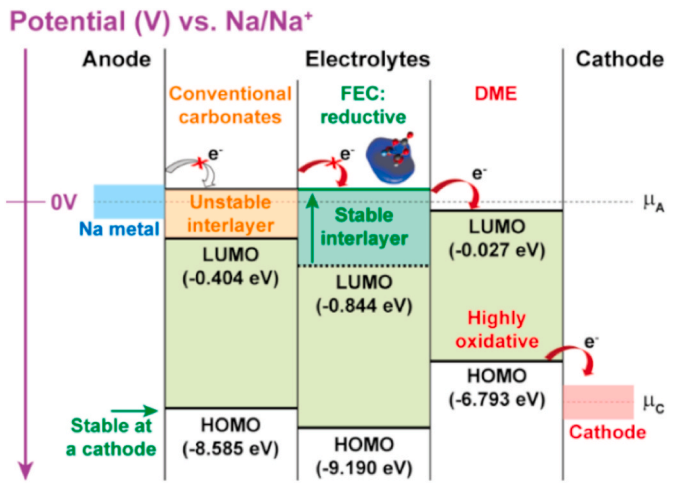

Fig. 22. HOMO-LUMO energy-level schematic diagram for DME, conventional carbonates and FEC additives. Reprinted with permission from Ref. [193] (Copyright © 2018, American Chemical Society).

industrial and commercial viability [195]. Consequently, it is imperative and significant to develop F-free electrolytes to realize the practical use of stable and long-term SMBs.

2.5.2.2. Nanostructured sodium anodes. ***Current collector/interlayer engineering.*** Homogenous Na plating can be realized by the 3D porous current collectors with the increased surface area to dissipate local current density *via* nanostructured engineering [196,197]. Recently, Luo et al. [198] demonstrated porous Al current collectors as the Na plating substrate to nucleate and reduce the Na^+ flux distribution, leading to uniform Na deposition without obvious protuberance/dendrites. They reported that the Na/porous Al anode ran over 1000 plating/stripping cycles with average CEs of 99.9 % and showed improved electrochemical performances compared to planar Al.

Additionally, the other approach to designing the nanostructured Na anodes is to construct a sodiophilic interlayer/interphase on the top of a Na metal anode for dendrite-free sodium nucleation and deposition behaviour. Very recently, Peng and co-workers [199] presented an oxygen-functionalized carbon nanotube network (O_f-CNTs) as the sodiophilic interphase on a Na anode, leading to an ultrahigh specific capacity of 1078 mAh g^{-1} and a long cycle life of 3000 cycles. They proposed that the O_f-CNTs network uniformly guided the Na nucleation behaviour and grew around the sodiophilic O-functional groups, endowing the Na@O_f-CNT with a dendrite-free morphology.

Nanostructured hosts of Na anodes. The 3D porous, sodiophilic and nanostructured host can accommodate the volume change during repeated plating/stripping processes to improve the electrochemical properties of sodium metal anodes [200,201]. Luo et al. [202] presented a mouldable and processable reduced graphene oxide (r-GO)/Na anode, illustrating enhanced strength and hardness as well as extended cycling stability in both carbonate and ether-based electrolytes due to the introduction of 4.5 wt% r-GO as the host. Furthermore, a Na@carbonized wood anode with porous and mechanically stable channels to confine the uniform Na nucleation has been fabricated by Hu et al. [203], showing the flat plating/stripping profiles over 500 h employed in carbonate electrolytes.

2.5.2.3. Separators optimization. To overcome the issues associated with the performance of SMBs, various strategies including the formulation and optimization of anode, cathode and electrolyte systems currently become research hotspots and the dominant direction by numerous researchers. However, the relevant studies on separator materials as a key component of batteries remain in the infancy stage compared to those regarding electrode and electrolyte materials of SMBs, indicating that the design and optimization of separators have been extensively neglected in the field of SMBs [179].

As one of the indispensable roles in metal batteries, the separator adequately blocks the contact between the cathode and anode while allowing the transport of ions in the electrolyte system through the separator [204]. The ideal separator enables enough mechanical strength to withstand the penetration of the dendrites, and simultaneously possesses enhanced thermal stability to circumvent the melting of the separator; otherwise, separator rupture and melting would ultimately cause the internal short circuit of the battery [205]. Currently, commercial Celgard (*i.e.*, monolayer polypropylene (PP), trilayer PP/polyethylene (PE)/PP membrane) and glass microfibre filter (GF) separators have been applied in SMBs but have inherent drawbacks, such as poor thermal stability of Celgard separators and unsatisfactory mechanical properties of GF separators [206]. Thus, growing attention and efforts should be devoted to designing and optimizing separators for improving the overall performance of safe-credible SMBs.

Modification of commercial separators. Zhou et al. [207] modified commercial Celgard PP separators with a single-ion-conducting polymer layer and the nitrogen-containing MXene coating *via* a grafting-filtering strategy, which suppressed Na dendrite growth, enhanced the wettability with carbonate-based electrolytes and cyclability of RT Na-S batteries. However, the modification procedure of commercial separators is complex and time/cost-consuming, which impedes the large-scale implementation of low-cost SMBs with chemically modified commercial separators.

Employment of new separators. Another selective method to restrain the Na dendrites formation in SMBs is to develop new appropriate separators to substitute the commercial-available ones. Xiang et al. [204] coated a paper-based membrane with graphitic carbon nitride (g-C_3N_4) *via* a dip-coating approach. They reported increased wettability, thermal stability, and ionic conductivity, as well as rate and cycling performances for a g-C_3N_4-coated paper-based separator in contrast with the conventional PE separator in SMBs. In addition, Kang et al. [208] fabricated a metastable γ-phase nylon-11 fibrous membrane by an electrospinning method with the 1,1,1,3,3,3-hexafluoro-2-propanol and trifluoroacetic acid (HFIP: TFA) solvent (see Fig. 23). They reported the stable stripping/plating cycling over 450 h at a current density of 0.5 mA cm^{-2} operated in 1 M NaPF6 in DME electrolytes.

Recently, Wang et al. [209] proposed a novel electrospun nanofibrous separator (*i.e.*, S-1000, S-3500) with uniaxially aligned nanofibres with a controllable alignment degree (see Fig. 24). Surprisingly, this unique S-3500 separator achieved stable and long-term cycling stability under high current densities (*i.e.*, ≥1000 h at 1 and 3 mA cm^{-2}, ≥700 h at 5 mA cm^{-2}) of SMBs operated in carbonate electrolytes without any additives.

These design schemes and strategies only enhanced the long-term cyclability of SMBs to some extent, and they are by far insufficient to meet the demand for the commercialisation of SMBs, particularly in carbonate-based electrolytes, which are the existing commercial and widely used choice for LIBs. It is noteworthy that most long-term stable sodium metal anodes are evaluated in ether-based electrolytes or fluorine-containing additives. Nevertheless, there are few reports about the long cycle life of SMBs in carbonate-based electrolytes without any additives. Therefore, it is a challenging area of research to achieve the long-term cycling stability of SMBs in low-cost carbonate-based electrolytes without any other additives *via* a simple or one-step and environmentally friendly strategy for large-scale applications of high-safety SMBs.

3. Conclusions and Outlook

This comprehensive review highlights the transformative potential of cellulose nanocrystals (CNCs) as sustainable and high-performance materials for next-generation sodium-ion, potassium-ion, and sodium-

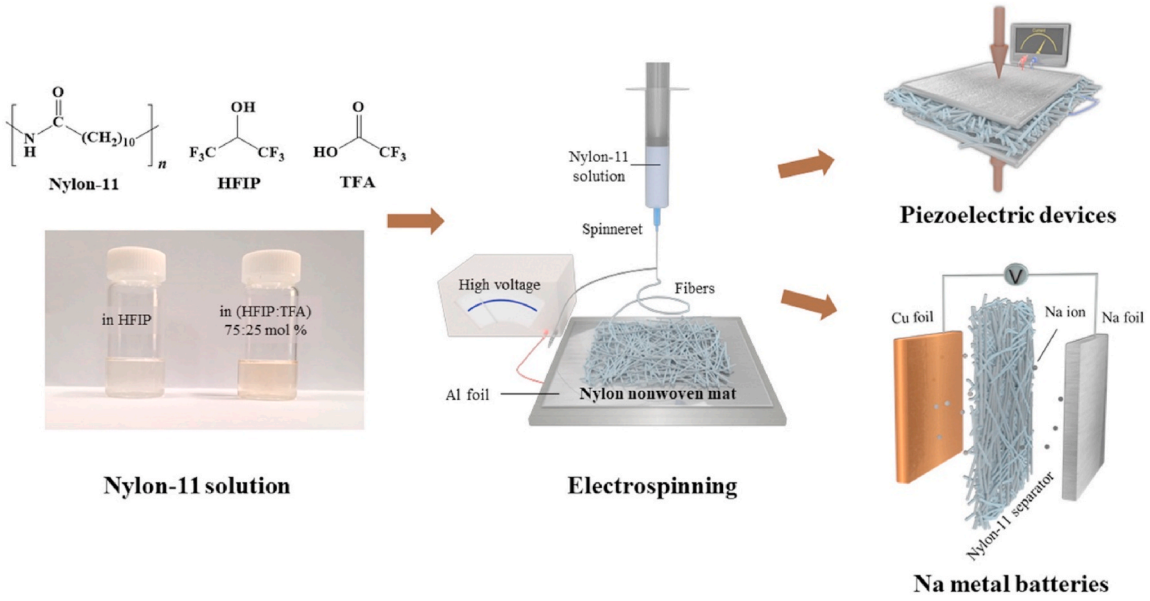

Fig. 23. Schematic illustrating the fabrication of a nylon-11 electrospun fibrous membrane and its employment as the separator for SMB or an active layer of a piezoelectric device. Reprinted with permission from Ref. [208] (Copyright © 2020, Elsevier).

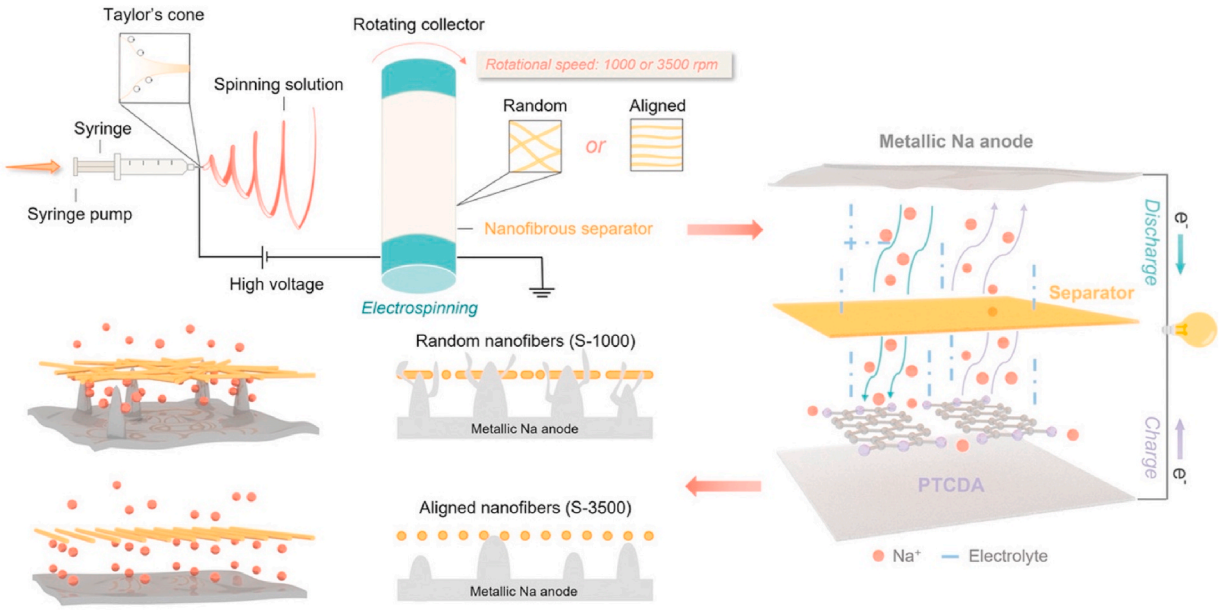

Fig. 24. Schematic of the fabrication of electrospun CNC/PEI nanofibrous membranes and Na deposition behaviours with S-1000 and S-3500 separators for Na-metal batteries. Reprinted with permission from Ref. [209] (CC-BY Open Access, 2022).

metal batteries. Leveraging the unique structural properties of CNCs, advanced fabrication techniques such as unidirectional ice-templating and precision electrospinning have enabled the development of highly aligned CNC-based nanocomposites with finely tailored electrochemical properties. These materials address critical challenges in conventional anode and separator design, including ion transport limitations and mechanical instability, while advancing environmental sustainability.

As post-lithium-ion battery technologies progress from laboratory exploration to industrial-scale implementation, CNC-based innovations stand poised to redefine the landscape of energy storage systems. The incorporation of aligned microstructures within CNC-based nanocomposites—ranging from electrodes to separators—offers a paradigm shift in achieving superior performance metrics such as cycling stability, energy density, and cost efficiency. By establishing systematic correlations between microstructure alignment and functional properties, this review provides a robust foundation for novel design strategies and inspires future research in sustainable energy storage. These above-mentioned works [145,209] both possess the additional merits of the sustainability of the precursors and scalable availability at comparatively low cost in a one-step fabrication process for electrodes and separators, which also offers design guidelines to be readily extended to a variety of other metallic (*e.g.*, Zn-, Al-, Ca-, Mg-)-based batteries for the large-scale commercialisation of energy storage technologies. By bridging material science, engineering, and sustainability, CNC-based innovations can accelerate the global shift toward carbon-neutral energy systems and redefine the future of energy storage for electric vehicles and grid applications.

The integration of scalable materials such as cellulose materials (*e.g.*,

CNCs) into advanced battery architectures represents a pivotal step toward sustainable energy storage solutions. Addressing key challenges, including the optimization of aligned microstructures to enhance ion transport and cycling stability, will require a concerted effort through interdisciplinary research and robust industrial collaborations. CNC-based nanocomposites hold immense potential as innovative separators and electrode materials, offering a path to cost-effective and high-performance sodium- and potassium-ion batteries and sodium-metal batteries. Technological advancements, containing scalable unidirectional ice-templating and high-speed electrospinning, are expected to bridge the gap between laboratory prototypes and commercial production. Moreover, the inherent biodegradability and renewable nature of CNCs align with sustainability goals. Recent strategies are highlighted to ensure the environmental footprint remains low during scale-up, such as using green solvents, energy-efficient processes, and recycling production by-products by developing life-cycle assessments (LCF) and environmental/techno-economic impact assessments *via* AspenPlus. By uniting material science, engineering innovation, and sustainability, advanced technologies are positioned to drive the global transition to carbon-neutral energy systems, reshaping the future of energy storage for electric vehicles and grid-scale applications.

While this review emphasizes sodium-/potassium-ion batteries and sodium-metal batteries, future research could explore CNC-based materials in other energy storage systems, such as lithium-sulfur or dual-ion batteries, to assess their versatility and potential to meet diverse energy demands. Furthermore, CNC-based nanocomposites could play a pivotal role in solid-state batteries (SSBs), where their mechanical flexibility and structural alignment may enhance ion transport and electrode/electrolyte interfaces. Research into CNC-based solid electrolytes or reinforced composite separators could open new pathways for SSB innovation. Emerging fabrication techniques (*e.g.*, 3D printing, additive manufacturing, roll-to-roll (R2R) processes) could be leveraged to create custom architectures for CNC-based electrodes and separators. These innovations would allow precise control over material alignment and porosity, optimizing battery performance.

Looking ahead, the application of sustainable nanocellulose or other biomass with precisely tailored aligned microstructures in all components (*i.e.,* hosts [210], electrodes, separators and electrolytes [211]) of anode-free batteries and SSBs presents a transformative opportunity [212]. These forward-looking perspectives aim to guide the research community toward innovative solutions and establish CNC-based batteries as a sustainable and high-performing alternative for next-generation energy storage applications. Consequently, these advancements promise the large-scale commercialisation of low-cost, high-performance, and environmentally sustainable energy-storage technologies, propelling the industry and society closer to achieving a net-zero emissions future.

CRediT authorship contribution statement

Jing Wang: Writing – review & editing, Writing – original draft, Visualization, Validation, Supervision, Software, Resources, Methodology, Investigation, Formal analysis, Data curation, Conceptualization. **Yue-E Miao:** Writing – review & editing, Writing – original draft, Formal analysis, Conceptualization.

Declaration of competing interest

The authors declare the following financial interests/personal relationships which may be considered as potential competing interests: Dr Jing Wang reports statistical analysis and writing assistance were provided by Swansea University. Dr Jing Wang reports a relationship with Swansea University that includes: employment. If there are other authors, they declare that they have no known competing financial interests or personal relationships that could have appeared to influence the work reported in this paper.

Appendix A. Supplementary data

Supplementary data to this article can be found online at https://doi.org/10.1016/j.coco.2025.102258.

Data availability

No data was used for the research described in the article.

References

[1] H.L. Van Soest, M.G. den Elzen, D.P. van Vuuren, Net-zero emission targets for major emitting countries consistent with the Paris Agreement, Nat. Commun. 12 (1) (2021) 1–9.
[2] N. Höhne, M.J. Gidden, M. den Elzen, F. Hans, C. Fyson, A. Geiges, M.L. Jeffery, S. Gonzales-Zuñiga, S. Mooldijk, W. Hare, Wave of net zero emission targets opens window to meeting the Paris Agreement, Nat. Clim. Change 11 (10) (2021) 820–822.
[3] U.N.E. Programme, Emissions Gap Report 2018, 2019. United Nations.
[4] U.N.E. Programme, Emissions Gap Report 2020, 2020. United Nations.
[5] N. Höhne, M. den Elzen, J. Rogelj, B. Metz, T. Fransen, T. Kuramochi, A. Olhoff, J. Alcamo, H. Winkler, S. Fu, Emissions: World Has Four Times the Work or One-Third of the Time, Nature Publishing Group, 2020.
[6] S.J. Davis, N.S. Lewis, M. Shaner, S. Aggarwal, D. Arent, I.L. Azevedo, S. M. Benson, T. Bradley, J. Brouwer, Y.-M. Chiang, Net-zero emissions energy systems, Science 360 (6396) (2018) eaas9793.
[7] H. Yaghoobnejad Asl, A. Manthiram, Toward sustainable batteries, Nat. Sustain. 4 (5) (2021) 379–380.
[8] B. Scrosati, J. Garche, Lithium batteries: status, prospects and future, J. Power Sources 195 (9) (2010) 2419–2430.
[9] A.R. Goldman, F.S. Rotondo, J.G. Swallow, Lithium Ion Battery Industrial Base in the US and Abroad, Institute for defense analyses, Alexandria VA, 2019.
[10] F. Duffner, M. Wentker, M. Greenwood, J. Leker, Battery cost modeling: a review and directions for future research, Renew. Sustain. Energy Rev. 127 (2020) 109872.
[11] M.S. Ziegler, J.E. Trancik, Re-examining rates of lithium-ion battery technology improvement and cost decline, Energy Environ. Sci. 14 (4) (2021) 1635–1651.
[12] F. Duffner, N. Kronemeyer, J. Tübke, J. Leker, M. Winter, R. Schmuch, Post-lithium-ion battery cell production and its compatibility with lithium-ion cell production infrastructure, Nat. Energy 6 (2) (2021) 123–134.
[13] L. Wang, Y. Liu, X. Du, X. Guo, Q. Zhao, Y. Wang, Z. Li, B. Liu, Z. Sun, Y. Men, W. Hu, Improved electrochemical properties of janus composite membranes obtained by modification of PEEK/nanocellulose on polyethylene for lithium-ion batteries, Compos. Commun. 40 (2023) 101624.
[14] W. Zhang, Y. Liu, Z. Guo, Approaching high-performance potassium-ion batteries *via* advanced design strategies and engineering, Sci. Adv. 5 (5) (2019) eaav7412.
[15] H. Kim, J.C. Kim, M. Bianchini, D.H. Seo, J. Rodriguez-Garcia, G. Ceder, Recent progress and perspective in electrode materials for K-ion batteries, Adv. Energy Mater. 8 (9) (2018) 1702384.
[16] X. Wu, Y. Chen, Z. Xing, C.W.K. Lam, S.S. Pang, W. Zhang, Z. Ju, Advanced carbon-based anodes for potassium-ion batteries, Adv. Energy Mater. 9 (21) (2019) 1900343.
[17] R. Usiskin, Y. Lu, J. Popovic, M. Law, P. Balaya, Y.-S. Hu, J. Maier, Fundamentals, status and promise of sodium-based batteries, Nat. Rev. Mater. 6 (11) (2021) 1020–1035.
[18] D. Su, G. Wang, Single-crystalline bilayered V2O5 nanobelts for high-capacity sodium-ion batteries, ACS Nano 7 (12) (2013) 11218–11226.
[19] I. Sultana, M.M. Rahman, Y. Chen, A.M. Glushenkov, Potassium-ion battery anode materials operating through the alloying–dealloying reaction mechanism, Adv. Funct. Mater. 28 (5) (2018) 1703857.
[20] H. Yang, R. Xu, Y. Yao, S. Ye, X. Zhou, Y. Yu, Multicore–shell Bi@ N-doped carbon nanospheres for high power density and long cycle life sodium-and potassium-ion anodes, Adv. Funct. Mater. 29 (13) (2019) 1809195.
[21] J.W. Choi, D. Aurbach, Promise and reality of post-lithium-ion batteries with high energy densities, Nat. Rev. Mater. 1 (4) (2016) 1–16.
[22] Z. Xu, J. Wang, Toward emerging sodium-based energy storage technologies: from performance to sustainability, Adv. Energy Mater. 12 (2022) 2201692.
[23] Z. Xu, Z. Guo, R. Madhu, F. Xie, R. Chen, J. Wang, M. Tebyetekerwa, Y.-S. Hu, M.-M. Titirici, Homogenous metallic deposition regulated by defect-rich skeletons for sodium metal batteries, Energy Environ. Sci. 14 (12) (2021) 6381–6393.
[24] D. Lin, Y. Liu, Y. Cui, Reviving the lithium metal anode for high-energy batteries, Nat. Nanotechnol. 12 (3) (2017) 194–206.
[25] K.-l. Hong, L. Qie, R. Zeng, Z.-q. Yi, W. Zhang, D. Wang, W. Yin, C. Wu, Q.-j. Fan, W.-x. Zhang, Biomass derived hard carbon used as a high performance anode material for sodium ion batteries, Journal of materials chemistry a 2 (32) (2014) 12733–12738.
[26] L. Xiao, Y. Cao, W.A. Henderson, M.L. Sushko, Y. Shao, J. Xiao, W. Wang, M. H. Engelhard, Z. Nie, J. Liu, Hard carbon nanoparticles as high-capacity, high-stability anodic materials for Na-ion batteries, Nano Energy 19 (2016) 279–288.
[27] F. Wu, L. Liu, Y. Yuan, Y. Li, Y. Bai, T. Li, J. Lu, C. Wu, Expanding interlayer spacing of hard carbon by natural K+ doping to boost Na-ion storage, ACS applied materials & interfaces 10 (32) (2018) 27030–27038.

[28] C. Xu, X. Yang, C. Hu, J. Zhang, L. Yang, S. Yin, One pot synthesis of polyoxometalate@polyaniline/MXene/CNTs quaternary composites with a 3D structure as efficient electrode materials for Li-ion batteries applications, Compos. Commun. 45 (2024) 101814.
[29] O. Aaltonen, O. Jauhiainen, The preparation of lignocellulosic aerogels from ionic liquid solutions, Carbohydr. Polym. 75 (1) (2009) 125–129.
[30] L. Heath, W. Thielemans, Cellulose nanowhisker aerogels, Green Chem. 12 (8) (2010) 1448–1453.
[31] Z. Ma, T. Xue, Q. Wali, Y.-E. Miao, W. Fan, T. Liu, Direct ink writing of polyimide/bacterial cellulose composite aerogel for thermal insulation, Compos. Commun. 39 (2023) 101528.
[32] Y. Habibi, L.A. Lucia, O.J. Rojas, Cellulose nanocrystals: chemistry, self-assembly, and applications, Chem. Rev. 110 (6) (2010) 3479–3500.
[33] S.J. Eichhorn, A. Dufresne, M. Aranguren, N.E. Marcovich, J.R. Capadona, S. J. Rowan, C. Weder, W. Thielemans, M. Roman, S. Renneckar, W. Gindl, S. Veigel, J. Keckes, H. Yano, K. Abe, M. Nogi, A.N. Nakagaito, A. Mangalam, J. Simonsen, A.S. Benight, A. Bismarck, L.A. Berglund, T. Peijs, Review: current international research into cellulose nanofibres and nanocomposites, J. Mater. Sci. 45 (1) (2010) 1–33.
[34] E.J. Foster, R.J. Moon, U.P. Agarwal, M.J. Bortner, J. Bras, S. Camarero-Espinosa, K.J. Chan, M.J.D. Clift, E.D. Cranston, S.J. Eichhorn, D.M. Fox, W.Y. Hamad, L. Heux, B. Jean, M. Korey, W. Nieh, K.J. Ong, M.S. Reid, S. Renneckar, R. Roberts, J.A. Shatkin, J. Simonsen, K. Stinson-Bagby, N. Wanasekara, J. Youngblood, Current characterization methods for cellulose nanomaterials, Chem. Soc. Rev. 47 (8) (2018) 2609–2679.
[35] A. Payen, Mémoire sur la composition du tissu propre des plantes et du ligneux, Comptes rendus 7 (lu 17 décembre 1838) (1838) 1052–1056.
[36] S.J. Eichhorn, A. Dufresne, M. Aranguren, N. Marcovich, J. Capadona, S. J. Rowan, C. Weder, W. Thielemans, M. Roman, S. Renneckar, Current international research into cellulose nanofibres and nanocomposites, J. Mater. Sci. 45 (1) (2010) 1–33.
[37] A.D. French, Glucose, not cellobiose, is the repeating unit of cellulose and why that is important, Cellulose 24 (11) (2017) 4605–4609.
[38] S.J. Eichhorn, Cellulose nanowhiskers: promising materials for advanced applications, Soft Matter 7 (2) (2011) 303–315.
[39] M.A.S. Azizi Samir, F. Alloin, A. Dufresne, Review of recent research into cellulosic whiskers, their properties and their application in nanocomposite field, Biomacromolecules 6 (2) (2005) 612–626.
[40] M. Mariano, N. El Kissi, A. Dufresne, Cellulose nanocrystals and related nanocomposites: review of some properties and challenges, J. Polym. Sci. B Polym. Phys. 52 (12) (2014) 791–806.
[41] A. Šturcová, I. His, D.C. Apperley, J. Sugiyama, M.C. Jarvis, Structural details of crystalline cellulose from higher plants, Biomacromolecules 5 (4) (2004) 1333–1339.
[42] J. Sugiyama, T. Okano, H. Yamamoto, F. Horii, Transformation of Valonia cellulose crystals by an alkaline hydrothermal treatment, Macromolecules 23 (12) (1990) 3196–3198.
[43] M.T. Postek, A. Vladár, J. Dagata, N. Farkas, B. Ming, R. Wagner, A. Raman, R. J. Moon, R. Sabo, T.H. Wegner, Development of the metrology and imaging of cellulose nanocrystals, Meas. Sci. Technol. 22 (2) (2010) 024005.
[44] H. Charreau, E. Cavallo, M.L. Foresti, Patents involving nanocellulose: analysis of their evolution since 2010, Carbohydr. Polym. 237 (2020) 116039.
[45] H. Kargarzadeh, M. Mariano, D. Gopakumar, I. Ahmad, S. Thomas, A. Dufresne, J. Huang, N. Lin, Advances in cellulose nanomaterials, Cellulose 25 (4) (2018) 2151–2189.
[46] T.C. Mokhena, M.J. John, Cellulose nanomaterials: new generation materials for solving global issues, Cellulose 27 (3) (2020) 1149–1194.
[47] E.J. Foster, R.J. Moon, U.P. Agarwal, M.J. Bortner, J. Bras, S. Camarero-Espinosa, K.J. Chan, M.J. Clift, E.D. Cranston, S.J. Eichhorn, Current characterization methods for cellulose nanomaterials, Chem. Soc. Rev. 47 (8) (2018) 2609–2679.
[48] H.A. Khalil, Y. Davoudpour, M.N. Islam, A. Mustapha, K. Sudesh, R. Dungani, M. Jawaid, Production and modification of nanofibrillated cellulose using various mechanical processes: a review, Carbohydr. Polym. 99 (2014) 649–665.
[49] O. Nechyporchuk, M.N. Belgacem, J. Bras, Production of cellulose nanofibrils: a review of recent advances, Ind. Crop. Prod. 93 (2016) 2–25.
[50] L. Chen, Q. Wang, K. Hirth, C. Baez, U.P. Agarwal, J. Zhu, Tailoring the yield and characteristics of wood cellulose nanocrystals (CNC) using concentrated acid hydrolysis, Cellulose 22 (3) (2015) 1753–1762.
[51] J. Wang, T.R. Pozegic, Z. Xu, R. Nigmatullin, R.L. Harniman, S.J. Eichhorn, Cellulose nanocrystal-polyetherimide hybrid nanofibrous interleaves for enhanced interlaminar fracture toughness of carbon fibre/epoxy composites, Compos. Sci. Technol. 182 (2019).
[52] S.A. Ogundare, W.E. van Zyl, A review of cellulose-based substrates for SERS: fundamentals, design principles, applications, Cellulose 26 (11) (2019) 6489–6528.
[53] R.J. Moon, A. Martini, J. Nairn, J. Simonsen, J. Youngblood, Cellulose nanomaterials review: structure, properties and nanocomposites, Chem. Soc. Rev. 40 (7) (2011) 3941–3994.
[54] D. Trache, A.F. Tarchoun, M. Derradji, T.S. Hamidon, N. Masruchin, N. Brosse, M. H. Hussin, Nanocellulose: from fundamentals to advanced applications, Front. Chem. 8 (2020).
[55] O.M. Vanderfleet, E.D. Cranston, Production routes to tailor the performance of cellulose nanocrystals, Nat. Rev. Mater. 6 (2) (2021) 124–144.
[56] R. Nickerson, J. Habrle, Cellulose intercrystalline structure, Ind. Eng. Chem. 39 (11) (1947) 1507–1512.
[57] B. Ranby, Aqueous Colloidal Solutions of Cellulose Micelles, Munksgaard Int Publ Ltd, COPENHAGEN, 1949, pp. 649–650, 35 NORRE SOGADE, PO BOX 2148, DK-1016.
[58] B.G. Rånby, Fibrous macromolecular systems. Cellulose and muscle. The colloidal properties of cellulose micelles, Discuss. Faraday Soc. 11 (1951) 158–164.
[59] S.M. Mukherjee, H.J. Woods, X-ray and electron microscope studies of the degradation of cellulose by sulphuric acid, Biochim. Biophys. Acta 10 (1953) 499–511.
[60] R.H. Marchessault, F.F. Morehead, N.M. Walter, Liquid crystal systems from fibrillar polysaccharides, Nature 184 (4686) (1959) 632–633.
[61] J.-F. Revol, H. Bradford, J. Giasson, R. Marchessault, D. Gray, Helicoidal self-ordering of cellulose microfibrils in aqueous suspension, Int. J. Biol. Macromol. 14 (3) (1992) 170–172.
[62] M. Roman, Toxicity of cellulose nanocrystals: a review, Ind. Biotechnol. 11 (1) (2015) 25–33.
[63] N. Grishkewich, N. Mohammed, J. Tang, K.C. Tam, Recent advances in the application of cellulose nanocrystals, Curr. Opin. Colloid Interface Sci. 29 (2017) 32–45.
[64] K.B. Teodoro, R.C. Sanfelice, F.L. Migliorini, A. Pavinatto, M.H. Facure, D. S. Correa, A review on the role and performance of cellulose nanomaterials in sensors, ACS Sens. 6 (7) (2021) 2473–2496.
[65] W. Zhang, X. He, C. Li, X. Zhang, C. Lu, X. Zhang, Y. Deng, High performance poly (vinyl alcohol)/cellulose nanocrystals nanocomposites manufactured by injection molding, Cellulose 21 (1) (2014) 485–494.
[66] S.H. Sung, Y. Chang, J. Han, Development of polylactic acid nanocomposite films reinforced with cellulose nanocrystals derived from coffee silverskin, Carbohydr. Polym. 169 (2017) 495–503.
[67] S. Huan, L. Bai, G. Liu, W. Cheng, G. Han, Electrospun nanofibrous composites of polystyrene and cellulose nanocrystals: manufacture and characterization, RSC Adv. 5 (63) (2015) 50756–50766.
[68] L. Rueda, A. Saralegui, B.F. d'Arlas, Q. Zhou, L.A. Berglund, M. Corcuera, I. Mondragon, A. Eceiza, Cellulose nanocrystals/polyurethane nanocomposites. Study from the viewpoint of microphase separated structure, Carbohydr. Polym. 92 (1) (2013) 751–757.
[69] N. Inai, A. Lewandowska, O. Ghita, S. Eichhorn, Interfaces in polyethylene oxide modified cellulose nanocrystal-polyethylene matrix composites, Compos. Sci. Technol. 154 (2018) 128–135.
[70] J.-E. Lee, Y.E. Kim, G.-H. Lee, M.J. Kim, Y. Eom, H.G. Chae, The effect of cellulose nanocrystals (CNCs) on the microstructure of amorphous polyetherimide (PEI)-based nanocomposite fibers and its correlation with the mechanical properties, Compos. Sci. Technol. 200 (2020) 108452.
[71] Z. Xue, D. He, X. Xie, Poly(ethylene oxide)-based electrolytes for lithium-ion batteries, J. Mater. Chem. A 3 (38) (2015) 19218–19253.
[72] S.A. Bagshaw, E. Prouzet, T.J. Pinnavaia, Templating of mesoporous molecular sieves by nonionic polyethylene oxide surfactants, Science 269 (5228) (1995) 1242–1244.
[73] J. Chen, S.K. Spear, J.G. Huddleston, R.D. Rogers, Polyethylene glycol and solutions of polyethylene glycol as green reaction media, Green Chem. 7 (2) (2005).
[74] W. Chen, Z. Xu, L. Yang, Electrochemical characteristics of bilayer film of polyaniline composite positive with polymer electrolyte binder/polymer electrolyte for Li-ion batteries, J. Power Sources 102 (1) (2001) 112–117.
[75] Y. Ito, M. Kawakubo, M. Ueno, H. Okuma, Q. Si, T. Kobayashi, K. Hanai, N. Imanishi, A. Hirano, M.B. Phillipps, Y. Takeda, O. Yamamoto, Carbon anodes for solid polymer electrolyte lithium-ion batteries, J. Power Sources 214 (2012) 84–90.
[76] Y. Liu, S. Gorgutsa, C. Santato, M. Skorobogatiy, Flexible, solid electrolyte-based lithium battery composed of LiFePO4 cathode and Li4Ti5O12 anode for applications in smart textiles, J. Electrochem. Soc. 159 (4) (2012) A349–A356.
[77] J. Sun, Y. Huang, W. Wang, Z. Yu, A. Wang, K. Yuan, Application of gelatin as a binder for the sulfur cathode in lithium–sulfur batteries, Electrochim. Acta 53 (24) (2008) 7084–7088.
[78] Y.-J. Choi, K.-W. Kim, H.-J. Ahn, J.-H. Ahn, Improvement of cycle property of sulfur electrode for lithium/sulfur battery, J. Alloys Compd. 449 (1) (2008) 313–316.
[79] S.-E. Cheon, J.-H. Cho, K.-S. Ko, C.-W. Kwon, D.-R. Chang, H.-T. Kim, S.-W. Kim, Structural factors of sulfur cathodes with poly(ethylene oxide) binder for performance of rechargeable lithium sulfur batteries, J. Electrochem. Soc. 149 (11) (2002) A1437–A1441.
[80] J.D. Beard, S.J. Eichhorn, Highly porous thermoplastic composite and carbon aerogel from cellulose nanocrystals, Mater. Lett. 221 (2018) 248–251.
[81] X. Xu, F. Liu, L. Jiang, J.Y. Zhu, D. Haagenson, D.P. Wiesenborn, Cellulose nanocrystals vs. cellulose nanofibrils: a comparative study on their microstructures and effects as polymer reinforcing agents, ACS Appl. Mater. Interfaces 5 (8) (2013) 2999–3009.
[82] T. Liu, Y. Tong, W.-D. Zhang, Preparation and characterization of carbon nanotube/polyetherimide nanocomposite films, Compos. Sci. Technol. 67 (3–4) (2007) 406–412.
[83] Z.-K. Xu, L.-Q. Shen, Q. Yang, F. Liu, S.-Y. Wang, Y.-Y. Xu, Ultrafiltration hollow fiber membranes from poly(ether imide): preparation, morphologies and properties, J. Membr. Sci. 223 (1) (2003) 105–118.
[84] M.K. Pitchan, S. Bhowmik, M. Balachandran, M. Abraham, Process optimization of functionalized MWCNT/polyetherimide nanocomposites for aerospace application, Mater. Des. 127 (2017) 193–203.

[85] K.S.Y. Lau, 10 - high-performance polyimides and high temperature resistant polymers, in: H. Dodiuk, S.H. Goodman (Eds.), Handbook of Thermoset Plastics, third ed., William Andrew Publishing, Boston, 2014, pp. 297–424.
[86] J. Wang, T.R. Pozegic, Z. Xu, R. Nigmatullin, R.L. Harniman, S.J. Eichhorn, Cellulose nanocrystal-polyetherimide hybrid nanofibrous interleaves for enhanced interlaminar fracture toughness of carbon fibre/epoxy composites, Compos. Sci. Technol. 182 (2019) 107744.
[87] K.L. Scotti, D.C. Dunand, Freeze casting – a review of processing, microstructure and properties via the open data repository, FreezeCasting.net, Prog. Mater. Sci. 94 (2018) 243–305.
[88] T. Moran, W.B. Hardy, The freezing of gelatin gel, Proc. R. Soc. Lond. - Ser. A Contain. Pap. a Math. Phys. Character 112 (760) (1926) 30–46.
[89] S. Deville, E. Saiz, R.K. Nalla, A.P. Tomsia, Freezing as a path to build complex composites, Science 311 (5760) (2006) 515–518.
[90] H. Zhang, I. Hussain, M. Brust, M.F. Butler, S.P. Rannard, A.I. Cooper, Aligned two-and three-dimensional structures by directional freezing of polymers and nanoparticles, Nat. Mater. 4 (10) (2005) 787–793.
[91] S. Bandi, M. Bell, D.A. Schiraldi, Temperature-responsive clay aerogel−polymer composites, Macromolecules 38 (22) (2005) 9216–9220.
[92] S.-M. Kwon, H.-S. Kim, H.-J. Jin, Multiwalled carbon nanotube cryogels with aligned and non-aligned porous structures, Polymer 50 (13) (2009) 2786–2792.
[93] J. Yang, W. Yang, W. Chen, X. Tao, An elegant coupling: freeze-casting and versatile polymer composites, Prog. Polym. Sci. 109 (2020) 101289.
[94] H. Joukhdar, A. Seifert, T. Jüngst, J. Groll, M.S. Lord, J. Rnjak-Kovacina, Ice templating soft matter: fundamental principles and fabrication approaches to tailor pore structure and morphology and their biomedical applications, Adv. Mater. 33 (34) (2021) 2100091.
[95] K.L. Scotti, D.C. Dunand, Freeze casting–A review of processing, microstructure and properties via the open data repository, FreezeCasting. net, Prog. Mater. Sci. 94 (2018) 243–305.
[96] L. Estevez, A. Kelarakis, Q. Gong, E.H. Da'as, E.P. Giannelis, Multifunctional graphene/platinum/nafion hybrids via ice templating, J. Am. Chem. Soc. 133 (16) (2011) 6122–6125.
[97] S.N. Schiffres, S. Harish, S. Maruyama, J. Shiomi, J.A. Malen, Tunable electrical and thermal transport in ice-templated multilayer graphene nanocomposites through freezing rate control, ACS Nano 7 (12) (2013) 11183–11189.
[98] B. Wicklein, A. Kocjan, G. Salazar-Alvarez, F. Carosio, G. Camino, M. Antonietti, L. Bergström, Thermally insulating and fire-retardant lightweight anisotropic foams based on nanocellulose and graphene oxide, Nat. Nanotechnol. 10 (3) (2015) 277–283.
[99] H. Shen, E. Yi, M. Amores, L. Cheng, N. Tamura, D.Y. Parkinson, G. Chen, K. Chen, M. Doeff, Oriented porous LLZO 3D structures obtained by freeze casting for battery applications, J. Mater. Chem. A 7 (36) (2019) 20861–20870.
[100] C. Stolze, T. Janoschka, S. Flauder, F.A. Müller, M.D. Hager, U.S. Schubert, Investigation of ice-templated porous electrodes for application in organic batteries, ACS applied materials & interfaces 8 (36) (2016) 23614–23623.
[101] H. Ma, H. Geng, B. Yao, M. Wu, C. Li, M. Zhang, F. Chi, L. Qu, Highly ordered graphene solid: an efficient platform for capacitive sodium-ion storage with ultrahigh volumetric capacity and superior rate capability, ACS Nano 13 (8) (2019) 9161–9170.
[102] Z. Xu, Y. Zhang, P. Li, C. Gao, Strong, conductive, lightweight, neat graphene aerogel fibers with aligned pores, ACS Nano 6 (8) (2012) 7103–7113.
[103] C. Adu, S. Rahatekar, J. Filby, D. Ayre, M. Jolly, Structural packaging foams prepared by uni-directional freezing of paper sludge cellulose nanofibres and poly (vinyl alcohol), Mater. Lett. 253 (2019) 242–245.
[104] B. Seantier, D. Bendahou, A. Bendahou, Y. Grohens, H. Kaddami, Multi-scale cellulose based new bio-aerogel composites with thermal super-insulating and tunable mechanical properties, Carbohydr. Polym. 138 (2016) 335–348.
[105] B.N. Nguyen, E. Cudjoe, A. Douglas, D. Scheiman, L. McCorkle, M.A.B. Meador, S. J. Rowan, Polyimide cellulose nanocrystal composite aerogels, Macromolecules 49 (5) (2016) 1692–1703.
[106] M.D. Gawryla, O. van den Berg, C. Weder, D.A. Schiraldi, Clay aerogel/cellulose whisker nanocomposites: a nanoscale wattle and daub, J. Mater. Chem. 19 (15) (2009).
[107] Y. Si, X. Wang, C. Yan, L. Yang, J. Yu, B. Ding, Ultralight biomass-derived carbonaceous nanofibrous aerogels with superelasticity and high pressure-sensitivity, Adv. Mater. 28 (43) (2016) 9512–9518.
[108] A. Formhals, United States: Patent Application Publication, vol. 1, US patent, 1934, p. 504, 1934.
[109] G.I. Taylor, Disintegration of water drops in an electric field, Proc. Roy. Soc. Lond. Math. Phys. Sci. 280 (1382) (1964) 383–397.
[110] D. Li, Y. Xia, Electrospinning of nanofibers: reinventing the wheel? Adv. Mater. 16 (14) (2004) 1151–1170.
[111] J. Xue, J. Xie, W. Liu, Y. Xia, Electrospun nanofibers: new concepts, materials, and applications, Accounts Chem. Res. 50 (8) (2017) 1976–1987.
[112] X. Li, W. Chen, Q. Qian, H. Huang, Y. Chen, Z. Wang, Q. Chen, J. Yang, J. Li, Y.-W. Mai, Electrospinning-based strategies for battery materials, Adv. Energy Mater. 11 (2) (2021) 2000845.
[113] D.H. Reneker, I. Chun, Nanometre diameter fibres of polymer, produced by electrospinning, Nanotechnology 7 (3) (1996) 216.
[114] M. Inagaki, Y. Yang, F. Kang, Carbon nanofibers prepared via electrospinning, Adv. Mater. 24 (19) (2012) 2547–2566.
[115] Z. Zhou, B. Chen, T. Fang, Y. Li, Z. Zhou, Q. Wang, J. Zhang, Y. Zhao, A multifunctional separator enables safe and durable lithium/magnesium–sulfur batteries under elevated temperature, Adv. Energy Mater. 10 (5) (2020) 1902023.
[116] X.H. Qin, S.Y. Wang, Filtration properties of electrospinning nanofibers, J. Appl. Polym. Sci. 102 (2) (2006) 1285–1290.
[117] R. Thakur, C. Florek, J. Kohn, B. Michniak, Electrospun nanofibrous polymeric scaffold with targeted drug release profiles for potential application as wound dressing, Int. J. Pharm. 364 (1) (2008) 87–93.
[118] D. Li, M.W. Frey, A.J. Baeumner, Electrospun polylactic acid nanofiber membranes as substrates for biosensor assemblies, J. Membr. Sci. 279 (1–2) (2006) 354–363.
[119] J. Xue, T. Wu, Y. Dai, Y. Xia, Electrospinning and electrospun nanofibers: methods, materials, and applications, Chem. Rev. 119 (8) (2019) 5298–5415.
[120] Y. Ju, H. Liu, Y. Chen, J. Sheng, Y. Zhai, B. Dong, R. Cheng, Y. Zhou, L. Li, An ultrathin Zn-BDC MOF nanosheets functionalized polyacrylonitrile composite separator with anion immobilization and Li+ redistribution for dendrite-free Li metal battery, Compos. Commun. 37 (2023) 101449.
[121] J.A. Matthews, G.E. Wnek, D.G. Simpson, G.L. Bowlin, Electrospinning of collagen nanofibers, Biomacromolecules 3 (2) (2002) 232–238.
[122] N. Narayanan, C. Jiang, G. Uzunalli, S.K. Thankappan, C.T. Laurencin, M. Deng, Polymeric electrospinning for musculoskeletal regenerative engineering, Regenerative Engineering and Translational Medicine 2 (2) (2016) 69–84.
[123] S.F. Fennessey, R.J. Farris, Fabrication of aligned and molecularly oriented electrospun polyacrylonitrile nanofibers and the mechanical behavior of their twisted yarns, Polymer 45 (12) (2004) 4217–4225.
[124] P. Katta, M. Alessandro, R. Ramsier, G. Chase, Continuous electrospinning of aligned polymer nanofibers onto a wire drum collector, Nano Lett. 4 (11) (2004) 2215–2218.
[125] Y. Song, L. Xu, Permeability, thermal and wetting properties of aligned composite nanofiber membranes containing carbon nanotubes, Int. J. Hydrogen Energy 42 (31) (2017) 19961–19966.
[126] L. Daelemans, S. van der Heijden, I. De Baere, H. Rahier, W. Van Paepegem, K. De Clerck, Using aligned nanofibres for identifying the toughening micromechanisms in nanofibre interleaved laminates, Compos. Sci. Technol. 124 (2016) 17–26.
[127] D. Li, A. Babel, S.A. Jenekhe, Y. Xia, Nanofibers of conjugated polymers prepared by electrospinning with a two-capillary spinneret, Adv. Mater. 16 (22) (2004) 2062–2066.
[128] Y. Xu, X. Liu, H. Su, S. Jiang, J. Zhang, D. Li, Hierarchical bimetallic selenides CoSe2–MoSe2/rGO for sodium/potassium-ion batteries anode: insights into the intercalation and conversion mechanism, Energy & Environmental Materials 5 (2) (2022) 627–636.
[129] C. Zhao, Q. Wang, Z. Yao, J. Wang, B. Sánchez-Lengeling, F. Ding, X. Qi, Y. Lu, X. Bai, B. Li, Rational design of layered oxide materials for sodium-ion batteries, Science 370 (6517) (2020) 708–711.
[130] W. Wang, J. Zhou, Z. Wang, L. Zhao, P. Li, Y. Yang, C. Yang, H. Huang, S. Guo, Short-range order in mesoporous carbon boosts potassium-ion battery performance, Adv. Energy Mater. 8 (5) (2018) 1701648.
[131] X. Shen, Q. Zhou, M. Han, X. Qi, B. Li, Q. Zhang, J. Zhao, C. Yang, H. Liu, Y.-S. Hu, Rapid mechanochemical synthesis of polyanionic cathode with improved electrochemical performance for Na-ion batteries, Nat. Commun. 12 (1) (2021) 1–10.
[132] H. Huang, R. Xu, Y. Feng, S. Zeng, Y. Jiang, H. Wang, W. Luo, Y. Yu, Sodium/potassium-ion batteries: boosting the rate capability and cycle life by combining morphology, defect and structure engineering, Adv. Mater. 32 (8) (2020) 1904320.
[133] W. Wang, B. Jiang, C. Qian, F. Lv, J. Feng, J. Zhou, K. Wang, C. Yang, Y. Yang, S. Guo, Pistachio-shuck-like MoSe2/C core/shell nanostructures for high-performance potassium-ion storage, Adv. Mater. 30 (30) (2018) 1801812.
[134] Z. Jian, Z. Xing, C. Bommier, Z. Li, X. Ji, Hard carbon microspheres: potassium-ion anode versus sodium-ion anode, Adv. Energy Mater. 6 (3) (2016) 1501874.
[135] L. Yue, J. Liang, Z. Wu, B. Zhong, Y. Luo, Q. Liu, T. Li, Q. Kong, Y. Liu, A.M. Asiri, Progress and perspective of metal phosphide/carbon heterostructure anodes for rechargeable ion batteries, J. Mater. Chem. A 9 (20) (2021) 11879–11907.
[136] J.-Y. Hwang, S.-T. Myung, Y.-K. Sun, Sodium-ion batteries: present and future, Chem. Soc. Rev. 46 (12) (2017) 3529–3614.
[137] Y. Mei, Y. Huang, X. Hu, Nanostructured Ti-based anode materials for Na-ion batteries, J. Mater. Chem. A 4 (31) (2016) 12001–12013.
[138] Y. Wen, K. He, Y. Zhu, F. Han, Y. Xu, I. Matsuda, Y. Ishii, J. Cumings, C. Wang, Expanded graphite as superior anode for sodium-ion batteries, Nat. Commun. 5 (1) (2014) 1–10.
[139] M.M. Doeff, Y. Ma, S.J. Visco, L.C. De Jonghe, Electrochemical insertion of sodium into carbon, J. Electrochem. Soc. 140 (12) (1993) L169.
[140] D. Stevens, J. Dahn, An in situ small-angle X-ray scattering study of sodium insertion into a nanoporous carbon anode material within an operating electrochemical cell, J. Electrochem. Soc. 147 (12) (2000) 4428.
[141] D. Stevens, J. Dahn, The mechanisms of lithium and sodium insertion in carbon materials, J. Electrochem. Soc. 148 (8) (2001) A803.
[142] J. Kim, M.S. Choi, K.H. Shin, M. Kota, Y. Kang, S. Lee, J.Y. Lee, H.S. Park, Rational design of carbon nanomaterials for electrochemical sodium storage and capture, Adv. Mater. 31 (34) (2019) 1803444.
[143] H. Zhu, F. Shen, W. Luo, S. Zhu, M. Zhao, B. Natarajan, J. Dai, L. Zhou, X. Ji, R. S. Yassar, Low temperature carbonization of cellulose nanocrystals for high performance carbon anode of sodium-ion batteries, Nano Energy 33 (2017) 37–44.
[144] Y. Feng, K. Wu, C. Xu, S. Wu, Z. Guo, M. He, X. Xu, M. Xue, Cellulose/lignin-based carbon nanobelt aerogels coating on VSe2 nanosheets as anode for high performance potassium-ion batteries, J. Power Sources 548 (2022) 232033.

[145] J. Wang, Z. Xu, J.-C. Eloi, M.-M. Titirici, S.J. Eichhorn, Ice-templated, sustainable carbon aerogels with hierarchically tailored channels for sodium- and potassium-ion batteries, Adv. Funct. Mater. 32 (16) (2022) 2110862.
[146] J. Liu, M. Cheng, Q. Liu, R. Wang, Y. Wei, W. Ma, J. Hu, T. Wei, Y. Ling, B. Liu, M. Chen, W. Li, Bimetallic Bi–Sn micro-/nanospheres@cellulose nanocrystal derived carbon aerogel composite anode for high-performance Mg-ion batteries, Compos. Commun. 39 (2023) 101553.
[147] Z. Wang, P. Tammela, M. Strømme, L. Nyholm, Cellulose-based supercapacitors: material and performance considerations, Adv. Energy Mater. 7 (18) (2017).
[148] H. Pan, X. Lu, X. Yu, Y.S. Hu, H. Li, X.Q. Yang, L. Chen, Sodium storage and transport properties in layered Na2Ti3O7 for room-temperature sodium-ion batteries, Adv. Energy Mater. 3 (9) (2013) 1186–1194.
[149] H. Li, H. Fei, X. Liu, J. Yang, M. Wei, In situ synthesis of Na 2 Ti 7 O 15 nanotubes on a Ti net substrate as a high performance anode for Na-ion batteries, Chem. Commun. 51 (45) (2015) 9298–9300.
[150] N. Yabuuchi, K. Kubota, M. Dahbi, S. Komaba, Research development on sodium-ion batteries, Chem. Rev. 114 (23) (2014) 11636–11682.
[151] H. Zhang, I. Hasa, S. Passerini, Beyond insertion for Na-ion batteries: nanostructured alloying and conversion anode materials, Adv. Energy Mater. 8 (17) (2018) 1702582.
[152] Y. Liu, Y. Xu, Y. Zhu, J.N. Culver, C.A. Lundgren, K. Xu, C. Wang, Tin-coated viral nanoforests as sodium-ion battery anodes, ACS Nano 7 (4) (2013) 3627–3634.
[153] P.R. Abel, Y.-M. Lin, T. de Souza, C.-Y. Chou, A. Gupta, J.B. Goodenough, G. S. Hwang, A. Heller, C.B. Mullins, Nanocolumnar germanium thin films as a high-rate sodium-ion battery anode material, J. Phys. Chem. C 117 (37) (2013) 18885–18890.
[154] A. Kohandehghan, K. Cui, M. Kupsta, J. Ding, E. Memarzadeh Lotfabad, W. P. Kalisvaart, D. Mitlin, Activation with Li enables facile sodium storage in germanium, Nano Lett. 14 (10) (2014) 5873–5882.
[155] Y. Kim, Y. Park, A. Choi, N.S. Choi, J. Kim, J. Lee, J.H. Ryu, S.M. Oh, K.T. Lee, An amorphous red phosphorus/carbon composite as a promising anode material for sodium ion batteries, Adv. Mater. 25 (22) (2013) 3045–3049.
[156] J. Sun, H.-W. Lee, M. Pasta, H. Yuan, G. Zheng, Y. Sun, Y. Li, Y. Cui, A phosphorene–graphene hybrid material as a high-capacity anode for sodium-ion batteries, Nat. Nanotechnol. 10 (11) (2015) 980–985.
[157] S. Yuan, X.l. Huang, D.l. Ma, H.g. Wang, F.z. Meng, X.b. Zhang, Engraving copper foil to give large-scale binder-free porous CuO arrays for a high-performance sodium-ion battery anode, Adv. Mater. 26 (14) (2014) 2273–2279.
[158] M. Valvo, F. Lindgren, U. Lafont, F. Björefors, K. Edström, Towards more sustainable negative electrodes in Na-ion batteries via nanostructured iron oxide, J. Power Sources 245 (2014) 967–978.
[159] L. Wang, K. Zhang, Z. Hu, W. Duan, F. Cheng, J. Chen, Porous CuO nanowires as the anode of rechargeable Na-ion batteries, Nano Res. 7 (2) (2014) 199–208.
[160] M.M. Rahman, I. Sultana, Z. Chen, M. Srikanth, L.H. Li, X.J. Dai, Y. Chen, Ex situ electrochemical sodiation/desodiation observation of Co 3 O 4 anchored carbon nanotubes: a high performance sodium-ion battery anode produced by pulsed plasma in a liquid, Nanoscale 7 (30) (2015) 13088–13095.
[161] L.-Y. Qi, Y.-W. Zhang, Z.-C. Zuo, Y.-L. Xin, C.-K. Yang, B. Wu, X.-X. Zhang, H.-H. Zhou, In situ quantization of ferroferric oxide embedded in 3D microcarbon for ultrahigh performance sodium-ion batteries, J. Mater. Chem. A 4 (22) (2016) 8822–8829.
[162] P.-F. Wang, Y. You, Y.-X. Yin, Y.-G. Guo, Layered oxide cathodes for sodium-ion batteries: phase transition, air stability, and performance, Adv. Energy Mater. 8 (8) (2018) 1701912.
[163] X. Zhang, X. Rui, D. Chen, H. Tan, D. Yang, S. Huang, Y. Yu, Na3V2(PO4)3: an advanced cathode for sodium-ion batteries, Nanoscale 11 (6) (2019) 2556–2576.
[164] W. Wang, Y. Gang, Z. Hu, Z. Yan, W. Li, Y. Li, Q.-F. Gu, Z. Wang, S.-L. Chou, H.-K. Liu, S.-X. Dou, Reversible structural evolution of sodium-rich rhombohedral Prussian blue for sodium-ion batteries, Nat. Commun. 11 (1) (2020) 980.
[165] H. Lyu, X.-G. Sun, S. Dai, Organic cathode materials for lithium-ion batteries: past, present, and future, Advanced Energy and Sustainability Research 2 (1) (2021) 2000044.
[166] C. Delmas, J.-J. Braconnier, C. Fouassier, P. Hagenmuller, Electrochemical intercalation of sodium in NaxCoO2 bronzes, Solid State Ionics 3 (1981) 165–169.
[167] P.F. Wang, Y. You, Y.X. Yin, Y.G. Guo, Layered oxide cathodes for sodium-ion batteries: phase transition, air stability, and performance, Adv. Energy Mater. 8 (8) (2018) 1701912.
[168] C.-l. Liu, S.-h. Luo, H.-b. Huang, Y.-c. Zhai, Z.-w. Wang, Layered potassium-deficient P2- and P3-type cathode materials KxMnO2 for K-ion batteries, Chem. Eng. J. 356 (2019) 53–59.
[169] Y. Huang, Y. Zheng, X. Li, F. Adams, W. Luo, Y. Huang, L. Hu, Electrode materials of sodium-ion batteries toward practical application, ACS Energy Lett. 3 (7) (2018) 1604–1612.
[170] M. Chen, W. Hua, J. Xiao, D. Cortie, W. Chen, E. Wang, Z. Hu, Q. Gu, X. Wang, S. Indris, NASICON-type air-stable and all-climate cathode for sodium-ion batteries with low cost and high-power density, Nat. Commun. 10 (1) (2019) 1–11.
[171] Z. Jian, C. Yuan, W. Han, X. Lu, L. Gu, X. Xi, Y.-S. Hu, H. Li, W. Chen, D. Chen, Y. Ikuhara, L. Chen, Atomic structure and kinetics of NASICON NaxV2(PO4)3 cathode for sodium-ion batteries, Adv. Funct. Mater. 24 (27) (2014) 4265–4272.
[172] Y. Li, Q. Zhou, S. Weng, F. Ding, X. Qi, J. Lu, Y. Li, X. Zhang, X. Rong, Y. Lu, Interfacial engineering to achieve an energy density of over 200 Wh kg− 1 in sodium batteries, Nat. Energy (2022) 1–9.
[173] J. Song, L. Wang, Y. Lu, J. Liu, B. Guo, P. Xiao, J.-J. Lee, X.-Q. Yang, G. Henkelman, J.B. Goodenough, Removal of interstitial H2O in hexacyanometallates for a superior cathode of a sodium-ion battery, J. Am. Chem. Soc. 137 (7) (2015) 2658–2664.
[174] W. Luo, M. Allen, V. Raju, X. Ji, An Organic pigment as a high-performance cathode for sodium-ion batteries, Adv. Energy Mater. 4 (15) (2014) 1400554.
[175] G. Zhou, Y.E. Miao, Z. Wei, L. Mo, F. Lai, Y. Wu, J. Ma, T. Liu, Bioinspired micro/nanofluidic ion transport channels for organic cathodes in high-rate and ultrastable lithium/sodium-ion batteries, Adv. Funct. Mater. 28 (52) (2018) 1804629.
[176] X. Han, C. Chang, L. Yuan, T. Sun, J. Sun, Aromatic carbonyl derivative polymers as high-performance Li-ion storage materials, Adv. Mater. 19 (12) (2007) 1616–1621.
[177] Y. Wang, Y. Wang, Y.-X. Wang, X. Feng, W. Chen, X. Ai, H. Yang, Y. Cao, Developments and perspectives on emerging high-energy-density sodium-metal batteries, Chem 5 (10) (2019) 2547–2570.
[178] P. Hartmann, C.L. Bender, M. Vračar, A.K. Dürr, A. Garsuch, J. Janek, P. Adelhelm, A rechargeable room-temperature sodium superoxide (NaO2) battery, Nat. Mater. 12 (3) (2013) 228–232.
[179] L. Ma, J. Cui, S. Yao, X. Liu, Y. Luo, X. Shen, J.-K. Kim, Dendrite-free lithium metal and sodium metal batteries, Energy Storage Mater. 27 (2020) 522–554.
[180] Y.-S. Hong, N. Li, H. Chen, P. Wang, W.-L. Song, D. Fang, In operando observation of chemical and mechanical stability of Li and Na dendrites under quasi-zero electrochemical field, Energy Storage Mater. 11 (2018) 118–126.
[181] L. Medenbach, C.L. Bender, R. Haas, B. Mogwitz, C. Pompe, P. Adelhelm, D. Schröder, J. Janek, Origins of dendrite formation in sodium–oxygen batteries and possible countermeasures, Energy Technol. 5 (12) (2017) 2265–2274.
[182] B. Sun, P. Xiong, U. Maitra, D. Langsdorf, K. Yan, C. Wang, J. Janek, D. Schröder, G. Wang, Design strategies to enable the efficient use of sodium metal anodes in high-energy batteries, Adv. Mater. 32 (18) (2020) 1903891.
[183] Y. Zhao, K.R. Adair, X. Sun, Recent developments and insights into the understanding of Na metal anodes for Na-metal batteries, Energy Environ. Sci. 11 (10) (2018) 2673–2695.
[184] A. Vyalikh, V.O. Koroteev, W. Münchgesang, T. Köhler, C. Röder, E. Brendler, A. V. Okotrub, L.G. Bulusheva, D.C. Meyer, Effect of charge transfer upon Li-and Na-ion insertion in fine-grained graphitic material as probed by NMR, ACS applied materials & interfaces 11 (9) (2019) 9291–9300.
[185] Y. Wang, H. Dong, N. Katyal, H. Hao, P. Liu, H. Celio, G. Henkelman, J. Watt, D. Mitlin, A sodium–antimony–telluride intermetallic allows sodium-metal cycling at 100% depth of discharge and as an anode-free metal battery, Adv. Mater. 34 (1) (2022) 2106005.
[186] C. Wang, L. Wang, F. Li, F. Cheng, J. Chen, Bulk bismuth as a high-capacity and ultralong cycle-life anode for sodium-ion batteries by coupling with glyme-based electrolytes, Adv. Mater. 29 (35) (2017) 1702212.
[187] Z.W. Seh, J. Sun, Y. Sun, Y. Cui, A highly reversible room-temperature sodium metal anode, ACS Cent. Sci. 1 (8) (2015) 449–455.
[188] V. Fleury, J.-N. Chazalviel, M. Rosso, Coupling of drift, diffusion, and electroconvection, in the vicinity of growing electrodeposits, Phys. Rev. 48 (2) (1993) 1279.
[189] C. Brissot, M. Rosso, J.N. Chazalviel, S. Lascaud, Dendritic growth mechanisms in lithium/polymer cells, J. Power Sources 81–82 (1999) 925–929.
[190] J. Lee, Y. Lee, J. Lee, S.-M. Lee, J.-H. Choi, H. Kim, M.-S. Kwon, K. Kang, K.T. Lee, N.-S. Choi, Ultraconcentrated sodium bis (fluorosulfonyl) imide-based electrolytes for high-performance sodium metal batteries, ACS Appl. Mater. Interfaces 9 (4) (2017) 3723–3732.
[191] R. Dugas, A. Ponrouch, G. Gachot, R. David, M.R. Palacín, J.-M. Tarascon, Na reactivity toward carbonate-based electrolytes: the effect of FEC as additive, J. Electrochem. Soc. 163 (10) (2016) A2333.
[192] M. Han, C. Zhu, T. Ma, Z. Pan, Z. Tao, J. Chen, In situ atomic force microscopy study of nano–micro sodium deposition in ester-based electrolytes, Chem. Commun. 54 (19) (2018) 2381–2384.
[193] Y. Lee, J. Lee, J. Lee, K. Kim, A. Cha, S. Kang, T. Wi, S.J. Kang, H.-W. Lee, N.-S. Choi, Fluoroethylene carbonate-based electrolyte with 1 M sodium bis (fluorosulfonyl) imide enables high-performance sodium metal electrodes, ACS applied materials & interfaces 10 (17) (2018) 15270–15280.
[194] Y. Lee, J. Lee, H. Kim, K. Kang, N.-S. Choi, Highly stable linear carbonate-containing electrolytes with fluoroethylene carbonate for high-performance cathodes in sodium-ion batteries, J. Power Sources 320 (2016) 49–58.
[195] J. Kim, J. Kim, J. Jeong, J. Park, C.-Y. Park, S. Park, S.G. Lim, K.T. Lee, N.-S. Choi, H.R. Byon, C. Jo, J. Lee, Designing fluorine-free electrolytes for stable sodium metal anodes and high-power seawater batteries via SEI reconstruction, Energy Environ. Sci. (2022).
[196] T.-S. Wang, Y. Liu, Y.-X. Lu, Y.-S. Hu, L.-Z. Fan, Dendrite-free Na metal plating/stripping onto 3D porous Cu hosts, Energy Storage Mater. 15 (2018) 274–281.
[197] M. Zhu, S. Li, B. Li, Y. Gong, Z. Du, S. Yang, Homogeneous guiding deposition of sodium through main group II metals toward dendrite-free sodium anodes, Sci. Adv. 5 (4) (2019) eaau6264.
[198] S. Liu, S. Tang, X. Zhang, A. Wang, Q.-H. Yang, J. Luo, Porous Al current collector for dendrite-free Na metal anodes, Nano Lett. 17 (9) (2017) 5862–5868.
[199] L. Ye, M. Liao, T. Zhao, H. Sun, Y. Zhao, X. Sun, B. Wang, H. Peng, A sodiophilic interphase-mediated, dendrite-free anode with ultrahigh specific capacity for sodium-metal batteries, Angew. Chem. 131 (47) (2019) 17210–17216.
[200] S.S. Chi, X.G. Qi, Y.S. Hu, L.Z. Fan, 3D flexible carbon felt host for highly stable sodium metal anodes, Adv. Energy Mater. 8 (15) (2018) 1702764.
[201] C. Wang, H. Wang, E. Matios, X. Hu, W. Li, A chemically engineered porous copper matrix with cylindrical core–shell skeleton as a stable host for metallic sodium anodes, Adv. Funct. Mater. 28 (30) (2018) 1802282.

[202] A. Wang, X. Hu, H. Tang, C. Zhang, S. Liu, Y.W. Yang, Q.H. Yang, J. Luo, Processable and moldable sodium-metal anodes, Angew. Chem. 129 (39) (2017) 12083–12088.
[203] W. Luo, Y. Zhang, S. Xu, J. Dai, E. Hitz, Y. Li, C. Yang, C. Chen, B. Liu, L. Hu, Encapsulation of metallic Na in an electrically conductive host with porous channels as a highly stable Na metal anode, Nano Lett. 17 (6) (2017) 3792–3797.
[204] L. Wu, X. Yao, Y. Liu, J. Ma, H. Zheng, X. Liang, Y. Sun, H. Xiang, A g-C3N4-coated paper-based separator for sodium metal batteries, J. Solid State Electrochem. 25 (4) (2021) 1373–1381.
[205] C.F. Francis, I.L. Kyratzis, A.S. Best, Lithium-ion battery separators for ionic-liquid electrolytes: a review, Adv. Mater. 32 (18) (2020) 1904205.
[206] W. Chen, L. Zhang, C. Liu, X. Feng, J. Zhang, L. Guan, L. Mi, S. Cui, Electrospun flexible cellulose acetate-based separators for sodium-ion batteries with ultralong cycle stability and excellent wettability: the role of interface chemical groups, ACS applied materials & interfaces 10 (28) (2018) 23883–23890.
[207] D. Zhou, X. Tang, X. Guo, P. Li, D. Shanmukaraj, H. Liu, X. Gao, Y. Wang, T. Rojo, M. Armand, Polyolefin-based janus separator for rechargeable sodium batteries, Angew. Chem. Int. Ed. 59 (38) (2020) 16725–16734.
[208] N.D.K. Tu, J. Park, S. Na, K.M. Kim, T.-H. Kwon, H. Ko, S.J. Kang, Co-solvent induced piezoelectric γ-phase nylon-11 separator for sodium metal battery, Nano Energy 70 (2020) 104501.
[209] J. Wang, Z. Xu, Q. Zhang, X. Song, X. Lu, Z. Zhang, A.J. Onyianta, M. Wang, M.-M. Titirici, S.J. Eichhorn, Stable sodium-metal batteries in carbonate electrolytes achieved by bifunctional, sustainable separators with tailored alignment, Adv. Mater. 34 (49) (2022) 2206367.
[210] X. Chen, Z. Yuan, J. He, L. Tong, Y. Wang, J. Wu, X. Li, Y. Chen, A lithiophilic MnO@biomass-derived carbon nanofiber host for stable lithium-metal batteries, Compos. Commun. 42 (2023) 101660.
[211] X. Song, K. Ma, H. Wang, J. Wang, J. Chen, Z. Zheng, J. Zhang, Enhancing Li+ transfer efficiency and strength of PEO-based composite solid electrolyte for long stable cycling of all-solid-state lithium metal batteries, Compos. Commun. 50 (2024) 102013.
[212] J. Wang, X. Han, Y. Feng, S. Chen, H. Yuan, R. Yang, W. Du, C. Hou, X. Liu, T. Tong, In-situ construction of a composite interlayer for dendrite-free Li6. 75La3Zr1. 75Ta0. 25O12 solid-state batteries, Compos. Commun. 46 (2024) 101851.